Máster en Astronomía y Astrofísica 2017-2018, 2ªconvocatoria

Predicción del PWV en el ORM: cuantificación de los valores óptimos para la Observación con CANARICAM. PWV forecasting at ORM: quantifying the best values to observe with CANARICAM

The shadow of the Roque de los Muchachos peak is projected over the sea of clouds as the Sun begins to rise in the opposite horizon. Photo: Gabriel Pérez

Gabriel Pérez Jordán, email: gabi@meteowhizz.com

Directora: Casiana Muñoz Tuñón (Instituto de Astrofísica de Canarias)

Table of contents

1. Abstract.
2. Scope and objectives.
3. The Canarian observatories: ORM and OT. The Gran Telescopio Canarias (GTC)
4. The Infrared Sky. Effect of atmospheric Precipitable Water Vapor and other molecules on IR observations. Observing in the mid-Infrared.
5. Gran Telescopio Canarias (GTC). Infrared instruments working at GTC.
6. CANARICAM.
7. Forecasting the PWV above the observatories in the Canary Islands: the FOR-O system.
8. Datasets and methods: PWV measured at ORM and CANARICAM observational data. Data analysis with the R statistical package.
9. Analysis and Results. CANARICAM observation log and PWV measurements by GPS monitor. CANARICAM measured sensitivity data. Results and discussion.
10. Summary and final conclusions. Future work.
11. References.
12. Acknowledgements.

1 Abstract

Observational time for instruments working in the infrared (IR) currently constitutes only a small fraction of the total available observational time in a telescope Schedule (e.g: 10%) in contrast with the available time for observations in the optical (visible) band. Therefore, optimization of such a scarce resource as this observational time for IR should be mandatory. Even observing a spectral line with its rest frame located in the optical, will lie in the infrared in the case of distant sources due to cosmological redshift. In this work we will explore the impact of Precipitable Water Vapour (PWV), the stronger absorber of IR radiation and thus the most critical parameter for instruments working in the infrared bands, for a specific instrument (CANARICAM) working in the mid-Infrared at the Gran Telescopio de Canarias (GTC). The absorption caused by PWV is not homogeneous through the infrared spectrum, with some spectral bands and lines more impacted than others. The ultimate goal is to determine the maximum value of PWV (PWV_{Max}) which allows observing with CANARICAM and finally obtain the expected probability of having this value (P_{PWVMax}) based on the long term (≈10 yr) PWV measurements from a GPS PWV monitor in operation at ORM. A set of equations is provided as a tool for estimating the expected sensitivity of the CANARICAM instrument as a function of PWV for the most used filters. In this context, knowing the current PWV conditions in real-time using the GPS PWV monitor and also its future evolution with the PWV forecasting system (For-O) in operation at the Canarian observatories becomes very important in terms of efficiency in the flexible (or service) mode of observations in the infrared at GTC.

Resumen

Actualmente el tiempo de observación dedicado a instrumentos trabajando en el infrarrojo (IR) contituye sólo una pequeña fracción del tiempo total de observación (p.ej: 10%) comparado con el tiempo disponible para observaciones en el óptico. Es por tanto muy importante optimizar el tiempo de observación en el IR. Incluso en observaciones de líneas espectrales con su longitud de onda en reposo en el óptico, aparecerán desplazadas hacia el infrarrojo para objetos distantes por efecto del desplazamiento al rojo cosmológico. En este trabajo, exploraremos el impacto del vapor de agua precipitable (PWV, por sus siglas en inglés), el parámetro con mayor impacto en los instrumentos que trabajan en el infrarrojo debido a su fuerte absorción, y más concretamente sobre CANARICAM, un instrumento que trabaja en el infrarrojo medio en el Gran Telescopio Canarias (GTC). La absorción causada por el PWV no es homogénea a los largo del

espectro infrarrojo, resultando algunas bandas o líneas espectrales más afectadas que otras. Nuestro objetivo es determinar el umbral máximo de PWV (PWV_{Max}) que permite observar con CANARICAM y obtener la probabilidad de que el PWV se mantenga por debajo de este valor máximo (P_{PWVMax}) basándonos en la serie climatológica (≈10 años) del PWV medido por el monitor GPS que realiza de forma rutinaria medidas del PWV en ORM. Presentamos un conjunto de ecuaciones como herramienta para la estimación de la sensitividad de CANARICAM en función del PWV para los filtros más utilizados en este instrumento. En este contexto, disponer de las condiciones de PWV en tiempo real a través del monitor GPS de PWV y conocer su evolución prevista usando el sistema de predicción de PWV (For-O) actualmente en servicio es muy importante en términos de eficiencia en el modo flexible (o servicio) de observaciones en el infrarrojo en GTC.

2 Scope and objectives

This work aims at providing a practical tool to determine the maximum Precipitable Water Vapour (PWV_{Max}) above the observatory which allows observing in the mid-Infrared (mid-IR) bands (N and Q) with the CANARICAM instrument given the two datasets: PWV measured locally at ORM with a GPS monitor and observational data directly obtained with the CANARICAM instrument at one of the Nasmyth focus of the Gran Telescopio de Canarias (GTC). We will go a little deeper proposing some criteria and equations to estimate the sensitivity depending on the PWV conditions and its evolution in the next hours or days, and on the IR filter(s) to be used for the observations based on previous flux and sensitivity measurements taken at GTC with CANARICAM.

Nowadays the amount of PWV is an observational constraint in most major observatories in the world, requiring the user to set a specific threshold not to be reached when applying for telescope time allocation. The problem is to know which PWV threshold must be specify depending on the IR instrument to be used and also on the science target. Using a “any” option value for PWV when requesting for telescope time could lead to invalid observations as the science target could not be detected (in the case of faint sources) if PWV value is above a certain threshold. Conversely, to give a too low PWV value without really needing it leads to an inefficient use of the telescope/instrument time that could be otherwise used by users/science

targets really in need of such low PWV. While the PWV is not really impacting observations below ~7500Å (i.e: at optical wavelenghts), at infrared (IR) wavelengths the selective absortion by atmospheric gases begins to be significant and in some bands the absorption is particularly effective, with greater impact at longer wavelengths (e.g: in the mid and far-infrared).

This work is structured as follows: chapter 3 gives a general vision of the location and characteristics of the canarian observatories and of Roque de los Muchachos Observatory (ORM) in particular. Chapter 4 explains the characteristics of the sky at IR wavelenghts, the impact the atmospheric gases have due to their radiative properties in the infrared and the particularities of observations at mid-infrared wavelengths. Chapter 5 is devoted to the new PWV forecasting system developed for the Instituto de Astrofísica de Canarias (IAC) which is delivering PWV forecasts above ORM and OT observatories four times a day since october 2018 and which complements the real-time PWV monitors based on the GPS technique in operation in both observatories. Chapter 6 briefly describes the GTC in the context of mid-infrared observations, introducing also the instruments working in the infrared bands at GTC. Chapter 7 explains CANARICAM in more detail. In chapter 8, the datasets used in the analysis are described. Chapter 9 presents the analysis and the results which are also discussed. Chapter 10 is a summary outlining the main conclusions and also, from these, we suggest the research lines to follow in future work.

3 The Canarian observatories: ORM and OT

The Roque de los Muchachos Observatory (ORM) and Teide Observatory (OT) are part of the The European Northern Observatory (ENO), one of the three most important geographical locations on Earth for Astronomy. A specific law (known as “Ley del cielo”) protects the skies of this unique locations from light pollution, radioelectric pollution, atmospheric pollution and also regulate air traffic routes above the observatories. The exceptional image quality of the Roque de los Muchachos, for example, has been documented since long (Muñoz Tuñón et al 1997, Hammersley 1998).

The ORM hosts the Gran Telescopio Canarias (GTC), one of the largest and most advanced optical-IR telescopes in the world. The telescope is located at about 2300 meters above sea level

in the Observatorio del Roque de los Muchachos (ORM) in the northern La Palma island (Canary Islands). A persistent temperature inversion originated by atmospheric subsidence exists throughout the year over the Canary Islands, located at subtropical latitudes, encouraging surface consistent tradewinds. This temperature inversion shows a marked seasonality with maximum frequency of occurrence during summer months and minima in winter (Dorta, 1996). The Canarian cold ocean current also contributes by cooling the air above the ocean surface. The combination of these two factors defines the subsidence inversion in the lower troposphere which helps to trap most of the water vapour below it maintaining usually very dry and transparent skies above. In addition, the night sky in La Palma island is protected by law against light pollution. Atmospheric water vapor decreases steadily in the vertical and most of the time it is confined in the first kilometers above the surface. This behaviour can be seen in figure 1 (left), which shows the average and median profiles of the water vapour mixing ratio obtained from a sample of 100 atmospheric radiosoundings launched from Tenerife. The presence of the inversion can also be seen at first sight through the stratocumulus cloud deck often present below the observatories, both located at about 2400 meters above sea level (figure 1 right).

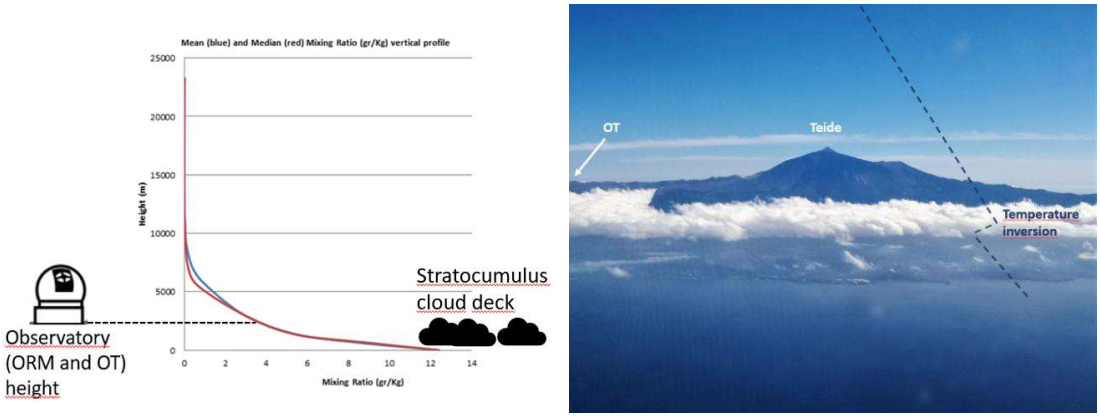

Figure 1. Vertical profile of the water vapour mixing ratio (left) obtained from a sample of 100 atmospheric soundings launched from Güímar (Tenerife island) and the temperature inversion in Tenerife made visible to the naked eye by the stratocumulus clouds that form from the base of the inversion. The same effect occurs at the neighboring island of La Palma, where ORM is located.

4 The Infrared Sky

In this chapter we do a brief review of the atmospheric transmission properties and the main sources of thermal background at infrared wavelengths. The central role of water vapour in infrared observations is also introduced with a deeper view into the mid-infrared.

4.1 Atmospheric Transmission. Infrared observation bands

While the Earth's atmosphere is relatively transparent to high frequency solar radiation, it can be almost opaque at certain wavelengths in the infrared. The reason for this lies in the fundamental structure of matter. The Earth's atmosphere is filled with gases in different abundances. It is mostly composed of molecular nitrogen (78% of the atmosphere's mass) and molecular oxygen (21% of the atmosphere's mass). However, the gases which are relevant in terms of absorption of radiant energy account for less tan 1% of the atmosphere's mass. This 1% is comprised of water vapour, carbon dioxide and ozone, among others.

Based on all the above, we can see that the transparency of the Earth's atmosphere is strongly variable with wavelength. An example of this behaviour is shown in figure 2, where the atmospheric transmission as a function of wavelength has been plotted for the range 1.5 to 2.4 microns, using ATRAN (Lord et al, 1992) software (available online at: https://atran.sofia.usra.edu/cgi-bin/atran/atran.cgi). Some features are easily seen in the figure: sets of absorption lines forming absorption bands, and wavelength ranges in which absortion is weak or inexistent, called "windows", in which observation is possible through custom designed filters. These windows have received special names in ground-based photometry and will be treated in greater detail in chapter 7. In figure 2 two of this near-infrared bands are shown, H (from 1.5 to 1.8 μm) and K (from 2.0 to 2.4 μm). The width, maximum transmission and the central wavelength of the windows show variations with geographical location and mainly, with altitude, due to its sensitivity to the water vapour content, as it will be further explained in the next section.

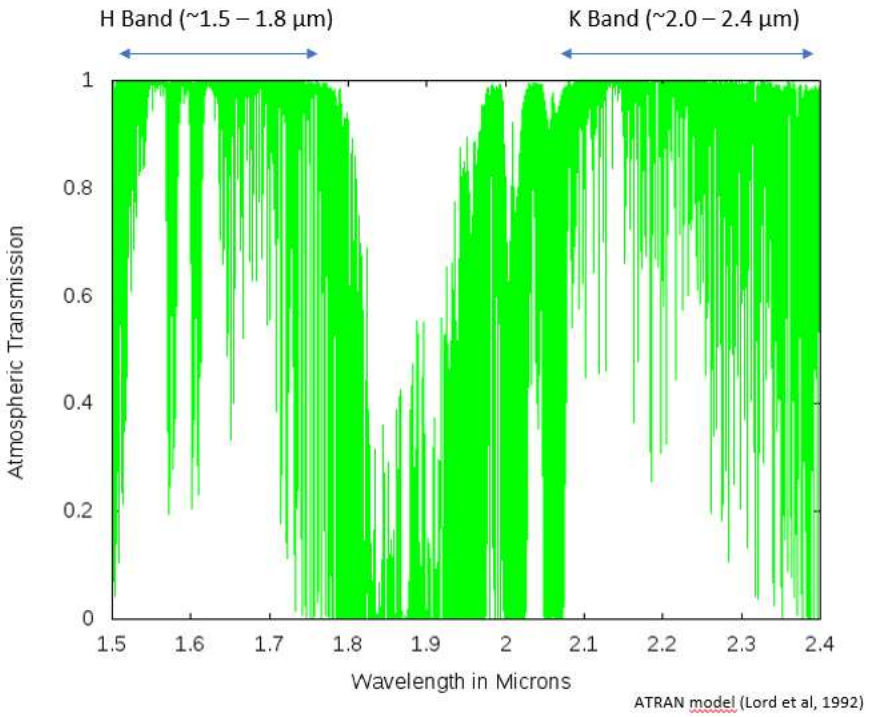

Figure 2. Plot of atmospheric transmission as a function of wavelength generated with ATRAN software, where the strongly variable behaviour of the atmosphere depending on the incoming radiation wavelength is apparent.

ATRAN is a computer atmospheric transmission model useful to compute a theoretical spectrum of atmospheric transmission (i.e: transmission as a function of wavelength). In this model all wavelengths are in vacuum. It was developed by Lord (1992) and its basic input parameters are described as follows and set to the indicated values to obtain the plot in figure 3 for the N band (mid-infrared):

- The observatory altitude in feet: we set it to 7874ft, that is, 2400m, the approx of ORM.
- The closest value of the observatory latitude: as the model only gives a few possibilities we select the closest available to ORM latitude which is 30ºN.
- Water Vapour Overburden at zenith: it must be given in microns, not millimeters as is PWV usually given (e.g: PWV=1mm equals 1000 microns).
- The number of atmospheric layers used in the model: usually is set to 2.
- Zenith angle of observations: we will consider observations at Airmass=1 so this field should be set to 0.

- Wavelength range (min and max) in microns, with min > 0.85: here we can select a specific bandwith to compute, for example, the atmospheric transmission in or near certain telluric lines. In ATRAN the maximum size of the wavelength range has been restricted to 60% of the central wavelength.
- Resolution R: the model spectrum will be smoothed with a Gaussian with a constant FWHM (Full Width at Half Maximum) value, where the FWHM is determined from the central wavelength of the spectrum divided by the resolution value R if one is specified. (A value of 0 for R means that no smoothing will be done.)

In this model one must take into account that the larger the wavelength range chosen, the longer it takes to perform the calculations. We have used ATRAN to obtain the spectrum of atmospheric transmission for each of the CANARICAM filters in both N and Q bands (mid-infrared) shown in figures 3 and 4.

4.2 Sources of absorption and background in the Infrared

Atmospheric Water Vapour

Although the Earth's atmosphere is composed of a large set of gases (N_2, O_2, CO_2, H_2O, O_3, among others), each with its own radiative properties and with variable proportions as a function of height, water vapour is the main absorber in the Earth's atmosphere at IR wavelenghts and also contributes to the thermal background. Water vapour in the atmosphere is closely tied to the distribution of temperature, so it is highly variable in space and time, and also with seasons. Water vapour content in the atmospheric column above one place, can be assessed through the Precipitable Water Vapour (PWV) value, defined as the total amount of water vapour contained in a vertical column of unit cross-sectional area from the surface to the top of the atmosphere. PWV is commonly expressed in mm, meaning the height that the water would reach if condensed and collected in a vessel of the same unit cross-section (American Meteorological Society, 2000). In general, water vapour content decreases rapidly with height, favouring those observatories located at high altitude . A single place in the Earth's surface can experiment large excursions in PWV, from ≈1 mm or below, to 15 mm or higher, even at places above 2000 meters. With such variability, the PWV becomes a very interesting variable to be

forecasted for astronomical observatories by, for example, a numerical weather prediction model, as will be shown in a real implementation in chapter 7. The PWV is a key variable specially for the world's biggest telescopes currently in operation, like GTC or VLT, or projected for the near generation of telescopes, as the ELT or TMT (Otárola et al, 2010).

Scattering

Air molecules and aerosols present in the atmosphere scatter incoming radiation thus contributing to the absorption at infrared wavelengths. Scattering causes atmospheric extinction (dimming of starlight by the terrestrial atmosphere). Two scattering mechanisms take place: Rayleigh and Mie scattering (Lockwood 2015). Rayleigh scattering refers to the elastic scattering produced by atomic and molecular particles whose diameter is less than the incoming radiation wavelength, so it is caused by the air molecules. Mie scattering refers to the elastic scattering caused by atomic or molecular particles whose diameter is larger than the incoming radiation wavelength, so it is caused mainly from aerosols, such as sea salts, hydrocarbons, wind-blown dust from deserts like the Sahara and volcanic dust. Its associated wavelength distribution depends on the size distribution of the aerosols. One key point regarding aerosols is that they can be found at very high altitude, so even astronomical sites located very high (like Mauna Kea, for example), are not free of this source of absorption. Measuring extinction requires observations at both low and high air masses so it is very time-consuming and not performed routinely but can be found in tabulated form for different infrared colours.

Zodiacal light

The zodiacal light is the dominant source of the mid-infrared sky brightness affecting ground-based observatories. It is associated with the dust present in the solar system, in particular, close to the plane of the planetary orbits (ecliptic). It is due to the direct emission from the dust particles and it varies with the Earth's position in its orbit around the Sun. It is very complex to model and substract. When comparing the zodiacal and exozodiacal (dust around other main sequence stars) spectra are very different. The exozodiacal spectra are dominated by cold dust, with emission peaking in the far-infrared, while the zodiacal spectrum peaks around 20 μm. In our case the Zodiacal light is not relevant due to the low latitude of ORM and OT observatories which keep the Zodiacal light close to the horizon.

4.3 Effect of atmospheric Precipitable water vapour and other atmospheric molecules on IR observations

The Earth's atmosphere behaves differently depending on the wavelenght of the radiation entering the atmosphere. For solar radiation, with wavelengths concentrated around 0.5 µm, the atmosphere is relatively transparent, whereas for infrared terrestrial radiation centered around 15 µm is becomes nearly opaque, so causing the well-known Earth's greenhouse effect.

Molecules or atoms in the atmosphere can be regarded as small oscillators, which have a discrete number of energy levels. The transition from one energy level to another corresponds to the release or capture of one photon of energy hv. The set of wavelengths at which one atmospheric molecule can absorb and/or emit photons results from a combination of energy storage modes: translational (or kinetic), rotational, vibrational and electronic energy. Each mode of energy storage involves a number of energies (which in turn correspond to the energy difference between two allowable states of the molecule). If a photon comes across the atmosphere with an energy which does not correspond to any allowed energy transitions of the many gas molecules which populate the atmosphere, it will pass through without being absorbed.

Translational energy is associated to the movement of molecules and is not quantized, but it plays an important role in broadening the range of wavelenghts at which radiation can be absorbed by an allowed transition between energy levels. The Doppler effect associated to this translational movements also contributes to broaden the range of wavelengths at which absorption or emission can take place associated to a energy transition in a gas molecule in the atmosphere.

The rotational energy is quantized and takes place at energy transition levels corresponding to wavelengths shorter than 1 cm. The vibrational energy is associated to the energy stored in the vibrations around the balance point in molecular bonds and is also quantized. This kind of energy transition requires the photon to have a wavelength of less than 20 µm. Each gas molecule can have independent modes of vibration (e.g: the CO_2 and N_2O molecules have 3 modes of vibration, 2 streching and 1 bending mode). During vibrational energy transitions, a molecule

can develop a temporal dipole moment which generates rotational transitions which add to the vibrational ones thus broadening the wavelenghts of absorption or emission creating an absorption band, for example.

The case of the water vapour molecule is very interesting: as it is a bent tri-atomic molecule, it has a permanent dipole moment which develops rotational transition bands which add to the vibration-rotation bands, causing it to be a very good absorber of IR radiation. The CO_2 molecule is another interesting case as its bending mode (vibration) is responsable for the strong vibration-rotation absorption feature at 15 µm. Water vapour has a important vibration-rotation band around 6.3 µm and a zone of dense rotational lines above ≈12 µm, leaving the spectrum between this two absorption features with relatively weak absorption so creating a "window" which constitutes the N band in mid-IR astronomy. As we will see later in chapter 6, many Canaricam filters take avantage of this atmospheric water vapour window.

One must take into account that atmospheric water vapour does not only absorb the incoming radiation but also increases the thermal IR background which in turn degrades the signal to noise (S/N) ratio in the detector.

4.3 Observing in the mid-Infrared

Infrared (IR) astronomy has become nowadays one of the most important and active lines in Astrophysics as it allows detection of many objects in our universe which are too faint or too cool to be detected in visible light (Glass, 1999). In the case of ground-based telescopes, mid-Infrared wavelengths suffer from high thermal sky backgrounds which in turn hinders observation of faint point sources and/or extended objects. While this is not a problem when observing from space, telescopes on board satellites are limited by size and weight so still there is an advantage when using infrared instruments in large ground-based telescopes, for example with primary mirror diameters of 8 to 10 meters. Large telescopes has the additional advantage when observing in the mid-infrared that the effect of seeing (resulting from atmospheric turbulence) is much less than at visible wavelenghts, especially at longer wavelengths (Q band), so diffraction limited images are obtained relatively easy. The diffraction limit of a telescope resolution is given by (Rayleigh criterion):

$$\theta_{arcsec} = 0.252\ \frac{\lambda\ (\mu m)}{a\ (m)}$$

where λ is the wavelength of interest in microns and a the telescope aperture in meters. In the case of the GTC and for the approximate central frequencies of both mid-IR bands N and Q we have:

$$\theta_{\text{arcsec}} = 0.26"$$

$$\theta_{\text{arcsec}\,Q} = 0.51"$$

Previous work has found little dependence between seeing (or Full Width at Half Maximum (FWHM)) and airmass at mid-IR wavelengths (Mason et al 2009).

The mid-Infrared technically covers from 5 to 25 µm, although the highest atmospheric trasmission occurs in two wide windows, namely the N and Q bands. The N band has a fairly good atmospheric transmission and covers from 8 to 14 µm approximately, with a strong absorption feature due to the presence of Ozone in the stratosphere at 9.6 µm (see figure 3). CANARICAM covers this whole band with a wide band filter (N-10.36) with a central wavelength of 10.36 µm and a bandwidth of 5.2 µm with a transmission of ≈80% across the whole band, and also specific sub-bands with medium and narrow-band filters.

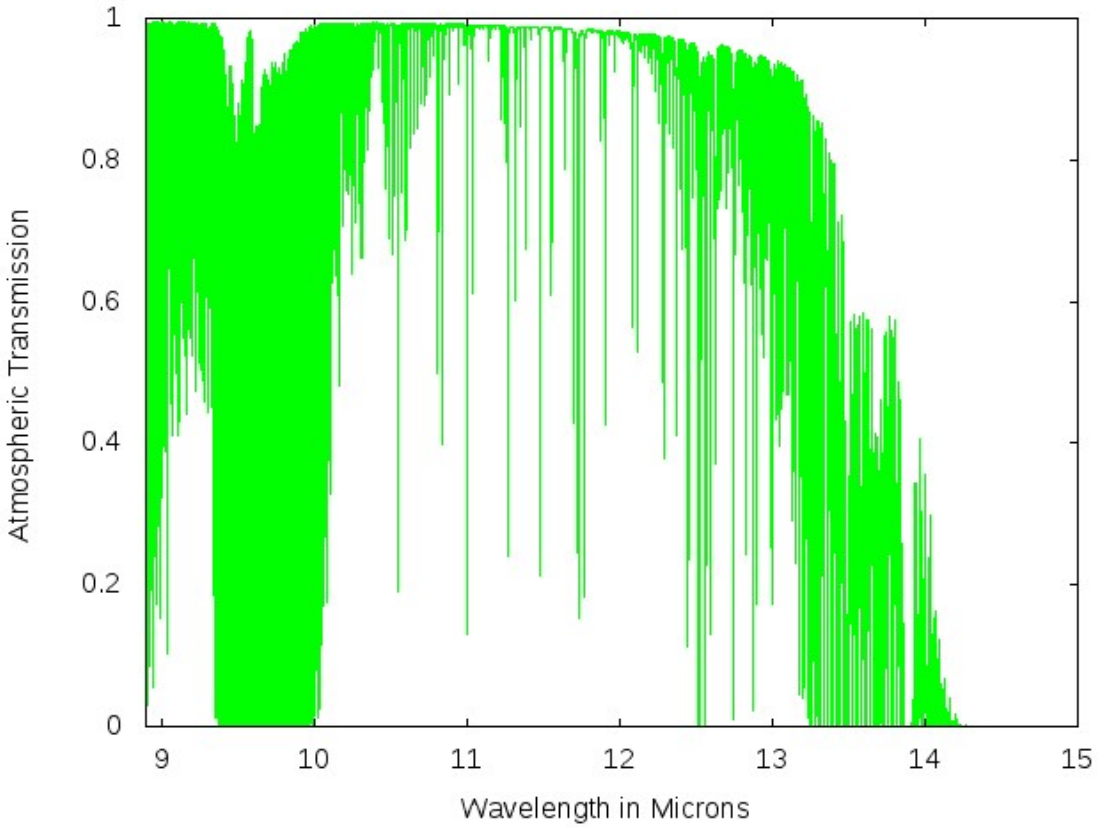

Figure 3. Plot of atmospheric transmission as a function of wavelength in the N band, generated with ATRAN software for an altitude of 2400 meters and 30º latitude (approximately the altitude and latitude of ORM and OT observatories), for a PWV of 3 mm above the observatories.

The Q band covers from 17 to 25 µm and is severely affected by water vapour, with increasing absoption with increasing wavelength for a fixed amount of PWV (see figure 4). CANARICAM covers this whole band with a wide band filter (Qw-20.8) with a central wavelength of 20.9 µm and a bandwidth of 8.8 µm with a transmission of ≈60% across the whole band and also with some specific médium and narrow-band filters.

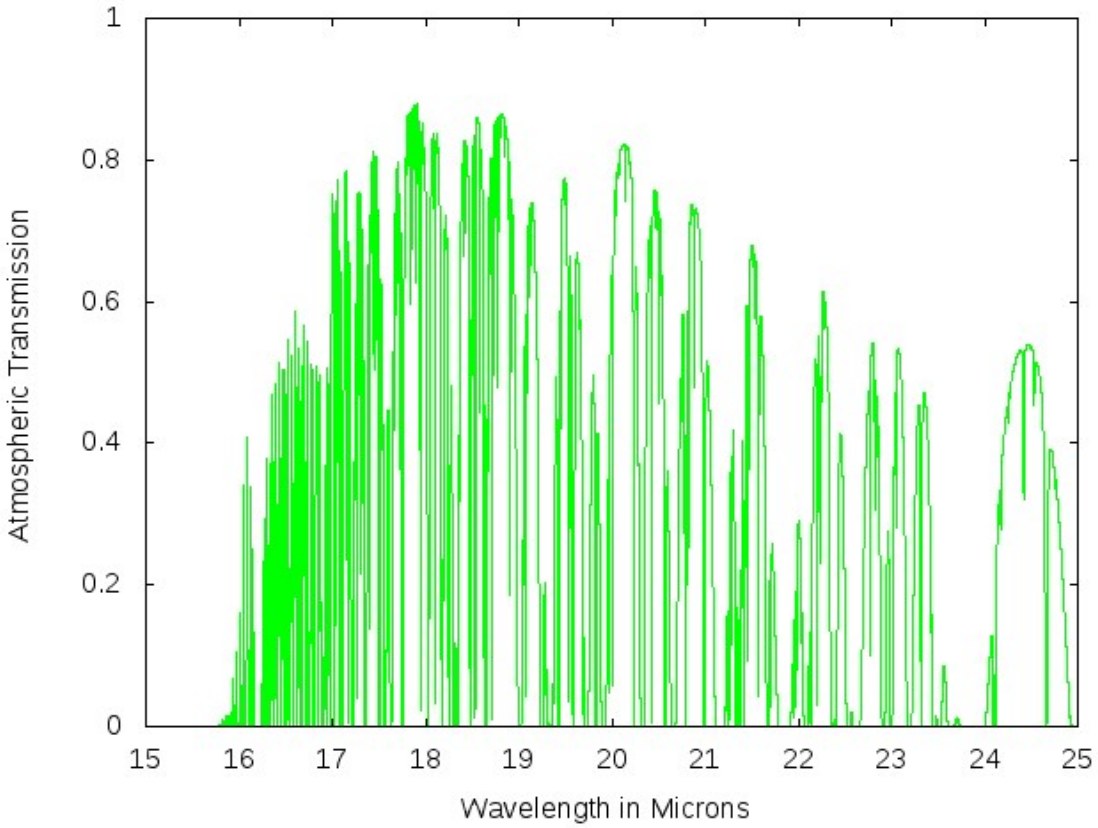

Figure 4. Plot of atmospheric transmission as a function of wavelength for the Q band generated with ATRAN software for an altitude of 2400 meters and 30º latitude (approximatelly the altitude and latitude of ORM and OT observatories), for a PWV of 3 mm above the observatories.

To overcome the high background typical at mid-IR wavelengths, the electronics in the detector play an essential role in doing the read out of the array as fast as possible before saturation. Ground-based telescopes must deal with background emission of typically 10^9 photons $s^{-1}\ m^{-2}\ \mu m^{-1}\ arcsec^2$ at λ≈10 μm while good typical detectors can have capacities (Full Well Capacity) of $\approx 3 * 10^7\ e^-$ in some arrays, like the one used in CANARICAM, so the read out speed becomes critical in the mid-infrared. To extract the huge background and make the science target "visible", a special technique known as *Chopping and Nodding* is used. In this technique, a stepwise-oscillating lightweight secondary mirror within the telescope, driven by actuators under feedback control, creates two positions (beams) in the sky, one containing the science target (source) and the other an empty piece of sky in the region of interest, close to the source, which are alternatively viewed by the detector at a high frequency, say 10 hz for example.

Substracting one signal from the other one can extract the science object from the background. Another background is nevertheless still present, the one generated by the telescope emissivity itself as the detector sees slightly different parts of the telescope structure as a result of the previous mechanism. This background is eliminated by moving the telescope with a frequency of some tens of seconds thus interchanging the images (source and empty sky) between the two beams so it can be substracted away.

4.4 Shift of Galaxy spectral features to the near-infrared (NIR) with redshift z

As a result of cosmological expansion, and thus the stretching of space-time, light arriving from distant objects tends to be shifted to longer wavelenghts. Although the observed redshift is a combination of the evolution of the metric and the peculiar motions due to variations in the comoving coordinate, only 10 out of a total of ~10^6 measured redshifts are negative (blueshifts) and correspond to objects in the local group or galaxies. Distances between objects in the Universe (proper distances) change in time due to variations of the scale factor (a) indepently of peculiar motions, which represent variations of the comoving distance. Another important observed property of redshift is its non-dependence with wavelength. Then, in this work we use the generally accepted explanation of measured redshifts as a result of the evolution of the metric of space-time, which in the framework of General Relativy (GR) is a result of the distribution of mass accross the Universe.

Redshift is defined as:

$$z = \frac{\lambda_0 - \lambda}{\lambda}$$

Where λ is the wavelength as measured of the spectral line in the laboratory and λ_0 is the wavelength of the same spectral line as observed in the Galaxy spectra. From the interpretation of the observed redshift as a change of the metric, the following expression results that relates z and wavelenghts λ and λ_0:

$$\frac{D_0}{D} = \frac{\lambda_0}{\lambda} = 1 + z$$

Where λ_0 is the wavelength of the light arriving from an object at time t_0 (now, at the time of observation, which is equivalent to the λ observed in the Galaxy spectra and thus affected by redshift) at a proper distance D_0 (when the scale factor is a_0) and λ is the wavelength at the time is was emitted (t, which is equivalent to the λ originally emitted, as in the laboratory, without being affected by redshift) when the scale factor was a and the proper distance was D. We have used this later equation to compute the position of the H_α spectral line at different redshifts. Spectral features in galaxies then appear redshifted with respect with the wavelength measured in the laboratory. This is the case, for example, of the rest frame Hα emission shown in figure 5, which is progresively shifted to redder wavelenghts as z increases.

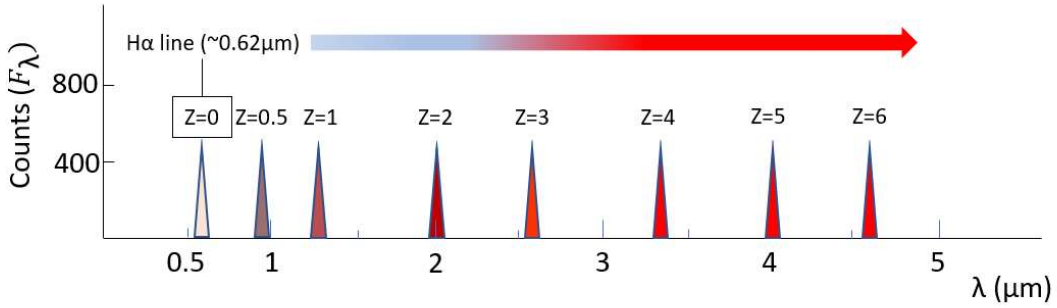

Figure 5. Effect of cosmological redshift of the source in the location of a particular spectral feature, like the Hα line. This same feature can be located all along the near-IR bands from 1 to almost 5 μm for increasingly distant galaxies.

This process reveals the fact that there will be some limitations when observing, for example, distant galaxies (i.e: for z>0.5) as the rest frame of the emission lines we are interested are located in the infrared, sometimes inside certain strong absorption bands.

We can use different emission lines to study specific sources, and then use one or another depending on redshift and on the atmosphere absorption at the particular wavelength in which

the emission line falls. In this sense, the seasonal distribution of PWV and the percentage of time in which the PWV is below a certain threshold is particularly useful. All this can be obtained from climatological data measured locally at ORM with the PWV GPS monitor, as will be shown later in chapter 10.

5 The telescope: Gran Telescopio Canarias (GTC). Telescope emissivity in the infrared. Infrared instruments working at GTC

5.1 The Gran Telescopio Canarias (GTC)

The Gran Telescopio Canarias (GTC) is nowadays one of the largest and most advanced optical-IR telescopes in the world. It started its production phase in 2009. 36 hexagonal segments, each one almost 2 meters across, form a perfectly hyperbolic light collecting area equivalent to a single monolithic primary mirror of 10.4 meters diameter. This mosaic mirror has the main advantage of being very light (is only eight centimetres thick and weights 470 kilograms; a similar monolithic mirror would weight nearly 17 tonnes) and thus suitable for implementation of an active optics system to correct for the atmospheric turbulence effects.

The GTC is a Ritchey-Chrétien design, thus with more complicated mirror surfaces capable of removing the coma (aberration typical of reflector telescopes, affecting images displaced from the optical axys, so that light rays does not converge into a point but form a kind of “comet” figure; hence the name “coma”. The coma has the effect of reducing the correct field of view) of the classical reflectors. It uses a hyperboloidal primary and secondary mirrors.

Currently the GTC incorporates an active optics system which allows the 36 segments to work as a single surface by means of sensors located at the edges of each segment which sends information to the central control system at a frequency of 20 Hz. In the near future (probably in 2019) GTC will have its own Adaptive Optics system (GTCAO), a technology that compensates for aberrations caused to light by atmospheric turbulence as it travels through the atmosphere by using deformable mirrors to apply real-time corrections (at a frequency of about 200 Hz).

Telescope emissivity in the infrared

The GTC itself is a source of infrared background specially at long wavelengths, as many structures that form and/or hold the primary (M1) and secondary (M2) mirrors can emit thermal radiation at mid-IR which affect the highly sensitive detector of CANARICAM. Some examples of such structures are: the telescope tube metallic structures around M1, the M2 metallic holding structure (both crearly seen in figure 12, left and right) and even the possible dust diposited on the mirror surface. Some actions have been taken in order to prevent this thermal emission entering CANARICAM, among others:

- A fraction of the primary mirror is vignetted in the secondary mirror to avoid the termal emission from the structures around M1 to enter CANARICAM.
- The physical separation between segments in M1 is minimized to 3 mm.
- M2 also has retractable baffles that cover unavoidable holes as the Cassegrain hole when observing in the optical, but leave them open to the sky during observations in the IR.
- To avoid the emission from the M2 supporting structures to enter the detector, CANARICAM has Lyot masks (cold masks that hides warm elements of the telescope within the pupil) that follow the shape of the GTC pupil.
- Mirror reflectivity is kept in maximum thus minimizing emissivity, by re-aluminization when required.
- CANARICAM offers a “imaging engineering mode” which allow to image the GTC pupil to make the necessary adjustments to minimize telescope emissivity.

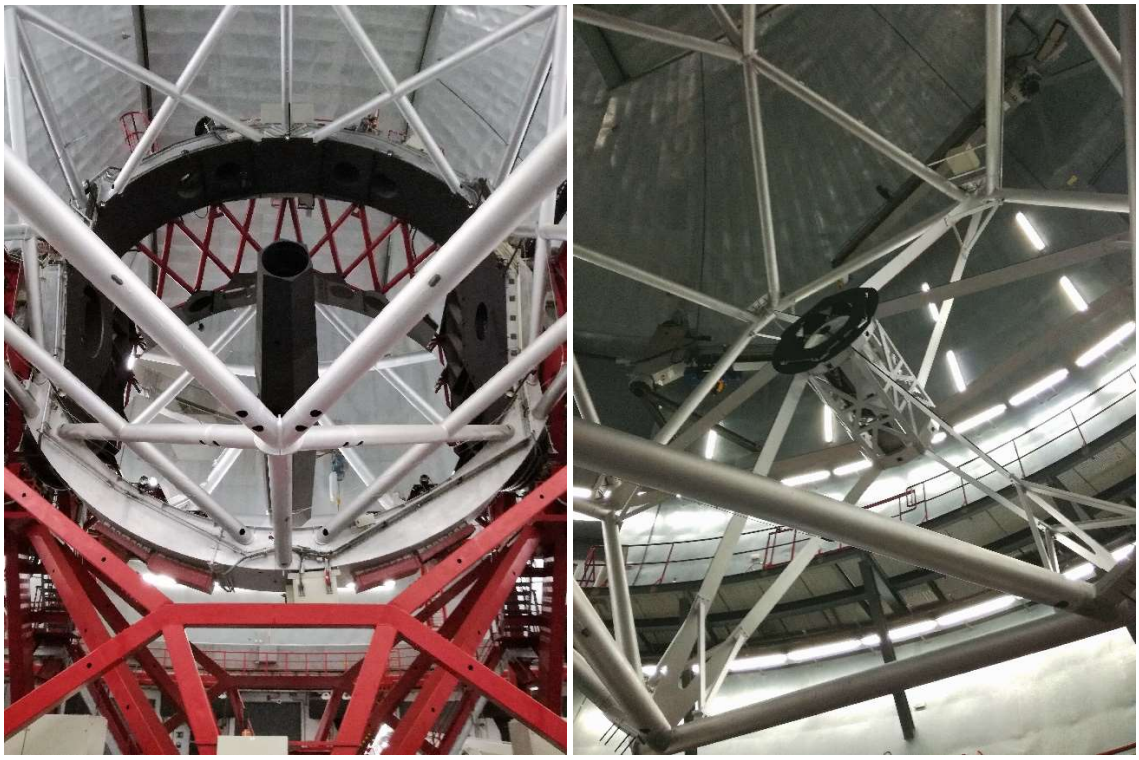

Figure 12. Some of the structures surrounding the primary (M1, left image) and secondary (M2, right image) mirrors in the GTC. Some measures have been taken to minimize the effect on the thermal background emission generated by such structures in order to prevent them from entering CANARICAM, and are explained in the text.

Observations at GTC are usually scheduled in queue mode. Observing time is offered to astronomers in Spain, Mexico and University of Florida. Moreover, once per year opportunities are opened for CCI International Time Programs (ITP). The observing time is offered issuing a call for proposals to which eligible astronomers should apply in order to be considered for observing time. These proposals are assessed and ranked on their scientific merit by the Time Allocation Committees (TACs) to decide which proposals will enter the observing schedule. But not only the scientific merit is assesed, but also the required observing conditions, the PWV amongst them, are key for a correct planning of observations. In queue-scheduled observing mode the observatory will take this into account and try to match the required observing conditions to the actual night observing conditions. Then usually observations are not given a fixed observing slot (or Observing Block, OB), but for equal scientific ranked proposals, the support astronomer puts into queue the one which better match the current conditions in what is called the flexible (or service) mode. The Observing Block (OB) is the minimum unit of observational time. OB's are

treated as atoms of a observing program and are normally not split in time. Long OB's are more difficult to schedule and more sensitive to variable observing conditions as well. The observatory only guarantees observation conditions for OB's, up to 1 hour. In GTC, a total overhead (extra time to be included inside the OB for calibrations, generation of flat fields and other tasks) of 10 minutes per OB should be accounted for.

When the weather conditions are such than any of the normal programs in the queue can be executed, the "filler" programs are then carried out. In the GTC website, the potential users of the telescope are reminded to not overstate their requirements for observing conditions. In this sense, our goal is to help researchers with some objetive criteria and tools to better specify the PWV requirement when applying for observing time with CANARICAM at GTC.

5.2 Infrared instruments and detectors working at GTC. EMIR, MIRADAS, GTCAO+FRIDA and CANARICAM.

The GTC hosts a wide variety of IR instruments which can be installed in the two Nasmyth foci (A and B) plus two-folded Cassegrain foci as well as in the main Cassegrain focus. The first infrared instrument for scientific use at GTC was CANARICAM, which started operation in 2012 after a long period of preparing the GTC for it, because of the need to implement the chopping technique used at infrared wavelenghts to overcome the huge background, which implies by an oscillating lightweight secondary mirror driven by actuators under feedback control. After four years of continuous operation, it was decomissioned in April 2016, but it will back to the GTC in Folded Cass E focus by the end of 2018.

EMIR is a near-infrared (0.9 - 2.5 μm) wide-field imager and medium-resolution multi-object spectrograph installed at the Naysmith-A focal station, which can obtain spectra of 55 objects simultaneously. MIRADAS is a near-IR multi-object echelle spectrograph with very high spectral resolution reaching R=20,000 over the whole spectral coverage, to be installed in late-2019 and becoming operational by early 2020. GTCAO+FRIDA combines the Adaptive Optics system for the GTC (GTCAO) with a near-IR hybrid imager and spectrograph. The arrival of GTCAO+FRIDA in 2019 will occupy the Nasmyth-B focal station.

Most IR instruments currently working at GTC cover the lower part of the near-IR bands (let's say, from 1 to 2.5μm), except in a specific instrument designed to observe in mid-IR

(CANARICAM). In this work we will focus on CANARICAM and thus in the mid-IR bands, but as long as PWV impact also the rest of the infrared spectrum, a brief description of some near-IR instruments is provided as follows. CANARICAM will be explained in more detail in chapter 9.

EMIR (Espectrógrafo Multiobjeto Infra-Rojo) is a near-infrared (0.9 - 2.5 µm) wide-field camera and medium-resolution multi-object spectrograph located at one of the Nasmyth focus. One of the main features of EMIR the possibility to configure and observe in real time up to 55 slits over the 4' x 6.67' spectroscopic field of view. Besides this, the user can configure also long slits with different dimensions. Its Field Of View (FOV) in imaging mode is 6.67' x 6.67' which can be observed through 11 narrow and broad-band filters, covering the atmospheric transmission windows in the 0.9 - 2.5 µm spectral rango (nea-IR), using the Y (1.03 µm), standard J (1.25 µm), H (1.63 µm), Ks (2.16 µm) 2MASS filters and Johnson K (2.23 µm) filter.

The 2048 x 2048 pixels (18 µm each) CCD is an evolution of the original NICMOS3 array, the most common in infrared astronomy, developed for the Hubble Space Telescope NICMOS instrument. It is based on a HgTeCd layer through which the incident radiation must pass. The detector surface is divided into 4 quadrants (1024 x 1024 pixels each) and these individual quadrants are read out through 8 channels, permitting a full frame rate of slightly over one frame per second as the 32 channels are read out simultaneously.

More details and additional information on EMIR can be found at:

http://www.gtc.iac.es/instruments/emir/

MIRADAS is a near-IR multi-object echelle spectrograph which allows simultaneous spectroscopy of up to 12 objects reaching spectral resolution of 20000. Its FOV is circular of 5 arcmin diameter with individual target FOV of 3.7 x 1.2 arcsec. MIRADAS covers many topics of research in modern infrared astrophysics as the detailed study of massive stars in our galaxy to help understand galactic structure and the chemical history of the Galaxy as well as studies of galaxies in our cosmic neighborhood, like the study of massive black holes at the centers of many of these galaxies. MIRADAS also has polarimetry capabilities which can be used in the study of

cirmumstellar disks, planet formation, and even the possibility of mapping the surface structures of cool stars.

http://www.gtc.iac.es/instruments/miradas/miradas.php

FRIDA (inFRared Imager and Dissector for Adaptive optics) performs a technique knows as "3D spectroscopy" combining its imaging and spectroscopy capabilities. It will work in the near-IR wavelength range and reaching spectral resolutions up to 30000. It will be the first instrument to make use of the GTC Adaptive Optics system.

More details and additional information on GTCAO+FRIDA can be found at:

http://www.gtc.iac.es/instruments/frida/

6 CANARICAM

6.1 CANARICAM description

CANARICAM is a field multimode camera and spectrograph operating in the mid-Infrared bands from 7.5 to 25 µm, with polarimetry and coronography capabilities (Telesco et al, 2003) and developed by the University of Florida specifically for the Gran Telescopio Canarias. It has been specially designed to work on the atmospheric windows in the N band, from 7 to 14 µm and in the Q band, from 17 to 25 µm. It is a special instrument as it works in a region of the infrared heavily impacted by the thermal background like the mid-IR, which has been traditionally difficult to observe from ground-based telescopes. The combination of the state-of-the-art technique and the privileged location of the ORM in terms of Precipitable Water Vapour makes observing at these long wavelenghts feasible when the PWV values move in a certain range. CANARICAM is a very unique instrument for the mid-infrared, as it combines classical model os observation like imaging and spectroscopy, to other not implement before at these wavelengths, as coronography and polarimetry.

The Detector

The detector is the common device used by all the CANARICAM modes of operation: imaging, spectroscopy, polarimetry and coronography. It is a Raytheon CRC-774 320x240 pixels Si:As (arsenic-doped silicon) Blocked Impurity Band (BIB) device, with a pixel scale of 0.08”/pixel, thus making a total Field Of View (FOV) of 25.6” x 19.2”. The array is made of two layered devices, the upper layer consisting in a highly infrared-sensitive material based on photoconductors or photodiodes, and the bottom layer is in charge of the array readout, and is called the *multiplexer*, built using conventional Silicon-based techniques (Glass, 1999). The detector’s Quantum Efficiency (QE) has a peak in the 8-25 μm region decreasing steadily for longer wavelengths. CanariCam raw images consist of a series of individual frames (savesets). The savesets are stored using multi-extension FITS files (MEF), which have the following structure:[320,240,2,M][N]. The first two fields represent the detector’s X and Y dimensions in pixels (320×240). The third field is the number of chop positions, called on-source and off-source positions. The fourth field, M, is the number of savesets in each nod position and N the number of nods (nod beams A and B). In the new future upgrade of CANARICAM for FCassE it will be considered a new detector readout management mode which would allow the storage of a higher number of independent readings in the so-called "burst mode" which increments data spatial resolution.

Canaricam science modes: imaging, spectroscopy, polarimetry and coronography

Imaging

It is considered the fundamental science mode of CANARICAM. Performing multi-wavelength mid-infrared imaging is posible to study the continuum emission of astronomical sources with temperatures in the 100-1000 K range, including dust, circumstellar disks, star-forming regions, starburst galaxies and AGN’s amongst others. I will allow to trace the distribution and temperatures of dust particles so gaining insight into the possible sources of energy that power the observed luminosities. Imaging with CanariCam is diffraction-limited at 8 μm over the full 25.6"x19.2" FOV and image distortion accross the FOV has been tested to be less than 2 pixels center-to-corner.

Spectroscopy

CANARICAM has four gratings, 2 working in the 10 µm (centered at 10.5 µm) and 2 in the 20 µm (centered at 20.5 µm) bands. In each band, one low resolution (with R between 120 and 175) and one high resolution (with R between 891 and 1313) are available. A slit wheel permits the selection of nine slits in the aperture wheel, so that one can match the slit width to the current seeing conditions and spectral resolution requirements. The spectrosopic mode allows the study of a wide range of solid-state and gas emission spectral features.

Polarimetry

CANARICAM has a dual-beam polarimetric mode for the 10 µm band which allows accurate polarimetry of bright sources during observing conditions that are too bad for almost any other type of observation. It is able to measure degrees of polarization as small as 0.1%. Polarimetry with CANARICAM makes possible to accurate mapping the magnetic alignment of dust particles in circumstellar disks, AGN's and young stellar objects and star-forming regions, among others. Polarimetry is a technique which allows to analyze the intensity and orientation of electromagnetic radiation, thus if the observed radiation is polarized with a given dependence on wavelength it is posible to obtain information about the physical mechanisms which produce the polarization. Regarding the PWV conditions, this observing mode is a little more demanding as temporal changes in atmospheric parameters such as PWV and seeing in scales of minutes may lead to wrong polarization results.

Coronography

This mode allows to suppress the stellar halo making posible the search for disks and faint stellar companions like planets. An occulting spot mask is inserted at the telescope focal plane and a pupil mask at the first pupil inside the camera.

Each science mode can be quickly selected during an observing sequence.

Observation with CANARICAM

When observing with CANARICAM some important points must be taken into account:

- As usual, Flat-field images must be generated for data reduction to correct fixed-pattern noise in the array, but as there is no standard method for obtaining accurate flat fields in the mid sensitivity-IR it must be almost customized for the instrument and telescope set-up. The problem arises from the fact that the screen mounted on the dome to obtain a uniform illumination of the detector for flat fields is a blackbody radiating at the room temperature, which will saturate the detector in almost all pass bands. Then usually a pair of flats are obtained with only a small percentage of variation between them which are later substracted to provide a map of spatial variations in sensitivity of the pixels across the array. This is important as inaccurate flat fields can leave residual fixed-pattern noise, or even worse, actually add noise and structure to the science data.

- The detection sensitivity of CANARICAM is very high, of 1 mJy for a 5-σ detection in a 1800 seconds on-source in imaging mode and 55 mJy equivalent in spectroscopy. This sensitiviy is maximized at 9 K and control of this temperature is critical because an increment of only ≈0.6K means a change in the detector's responsivity of ≈30%. When changing filters is normal that temperature variations occur so the operator must wait until the temperature reaches its operating value again before starting observations.

6.2 Filters used in CANARICAM

The CANARICAM filter suite for both mid-IR bands (10 and 20 µm) are located in two filter wheels after the Lyot-stop wheel at the first pupil image. CANARICAM has 6 medium-band silicate filters (Si1 through Si6) and 13 narrow, medium and wide band filters. Aside from these, there are two specific filters to be used in Spectroscopy: Lowres10 (in the 10 µm band) band) and Lowres20 (in the 20 µm). These two low resolution gratings are one spanning 7.4-13.5 µm and the other spanning 15.7-25.3 µm. Next table shows all filters available in CANARICAM, with its central wavelength ($\lambda_{central}$) and bandwidth (Δλ):

Filter	$\lambda_{central}$ (μm)	Δλ (μm)
Si1-7.8	7.8	1.1
PAH1-8.6	8.6	0.43
Si2-8.7	8.7	1.1
ArIII-8.99	8.99	0.13
Si3-9.8	9.8	1.0
Si4-10.3	10.3	0.9
N-10.36	10.36	5.2
SIV-10.5	10.51	0.16
PAH2-11.3	11.3	0.6
Si5-11.6	11.6	0.9
SiC-11.75	11.75	2.5
Si6-12.5	12.5	0.7
NeII-12.8	12.8	0.2
NeII_ref2-13.1	13.1	0.2
QH2-17.0	17.0	0.4
Q1-17.65	17.65	0.9
Q4-20.5	20.5	1.0
Qw-20.8	20.8	8.8
Q8-24.5	24.5	0.8

Figure 13 show the transmission curves of all filters available in Canaricam (green curves) and the theoretical trasmission of the atmosphere with its absorption features due to presence of gases with diferente radiative properties, for both N and Q bands obtained with ATRAN model. Some interesting features are visible in both plots:

- The N and Q mid-IR bands are “separated” by the strong absorption feature of CO_2 near 15 μm.

- A strong absorption band falls around 9.6 μm, caused by Ozone. Canaricam narrowband filters near this wavelentgth avoid this absoption feature, while wider filter (as the Si3) include them as there are still good atmospheric transmission at wavelengths close to 9.6 μm. This filter (Si3) centered close to this absorption feature, is not commonly used.

- A strong dependence of atmospheric transmission on wavelength is clearly seen in the red curve (theoretical atmospheric transmission obtained with the ATRAN model) in

figure 13, with the higher (redder) wavelengths much more affected and rapidly decreasing transmission for the same amount of PWV above the observatory.

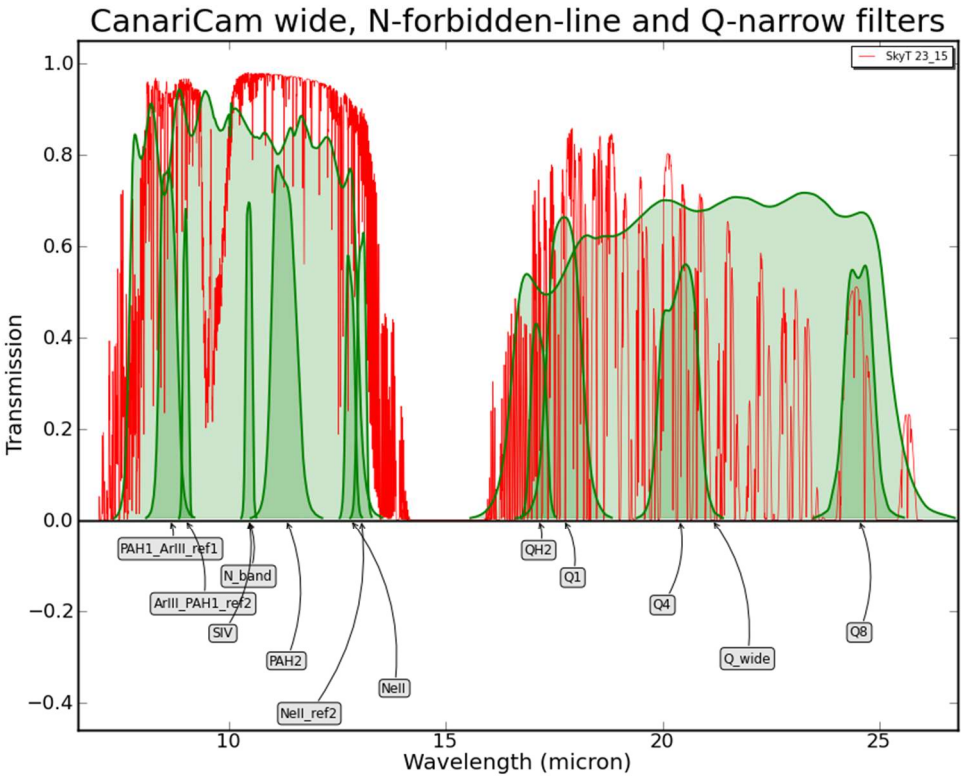

Fig 13 Plot of transmission as a function of wavelength in the mid-Infrared region, with CANARICAM's broad-band N (N_band) and Q (Q_wide), narrow-band 20-micron (QH2, Q1, Q4 and Q8) and forbidden-line narrow-band 10 µm filters (PAH1, PAH2, NeII, NeII_ref2, SIV and ArIII). The theoretical atmospheric transmission obtained with ATRAN model for a PWV amount of 2.3 mm and Airmass 1.5, is shown in red. Figure courtsey of GTC (http://www.gtc.iac.es)

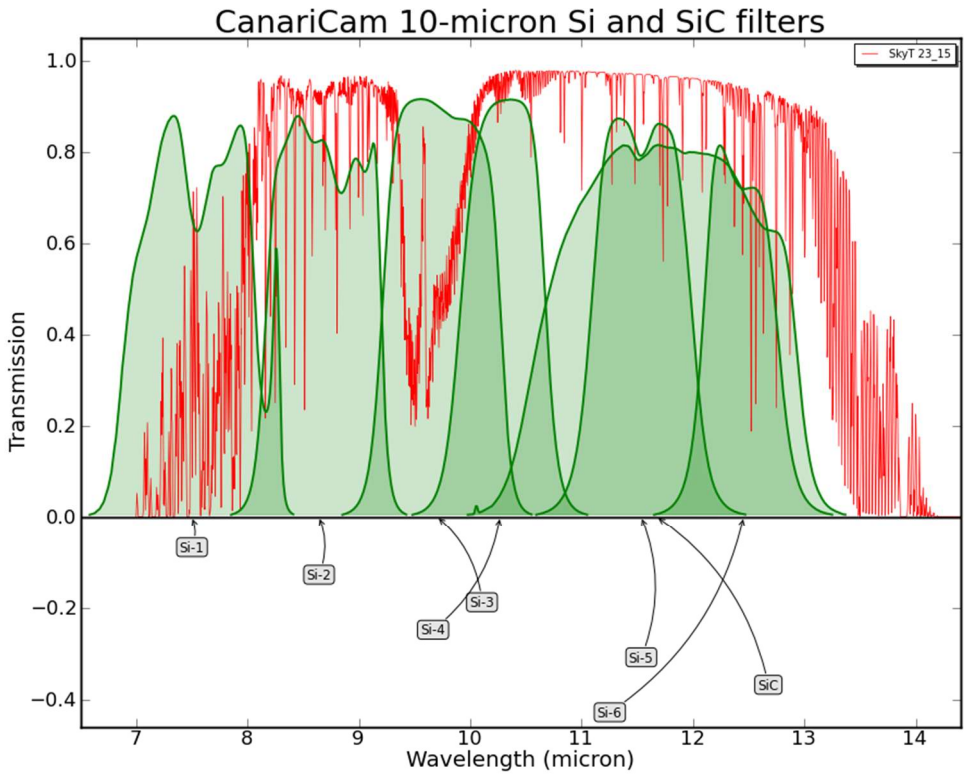

Fig 14. Same as Fig.13, but for CANARICAM's medium-band Silicate filters (Si1 through Si6) and wide band SiC. Again, the theoretical atmospheric transmission obtained with ATRAN model for a PWV amount of 2.3 mm and Airmass 1.5, is shown in red. Figure courtsey of GTC (http://www.gtc.iac.es)

6.3 CANARICAM tools: the Exposure Time Calculator

Principal investigators (PI) requesting observing time for CANARICAM must follow a process in two phases using a web-based GTC application. In phase 2 of that process, they must specify a detailed as possible description of his/her observations and that includes the observing conditions. PI's can use a specific tool for CANARICAM, the Exposure Time Calculator (or ETC). In the ETC There are two modes available for Imaging:

- Calculate the total SNR resulting from a user specified on-source integration time (in seconds)

- Calculate the on-source integration time to achieve a user specified SNR.

For spectroscopy only the former mode is available due to as the SNR can vary markedly with wavelength specially in the mid-infrared. The user must specify the observing conditions constrains: image quality, cloud cover, PWV, sky background and airmass.

Regarding the PWV, the user can choose among certain percentiles (20%, 50% (median), 80% or ANY) indicating the frequency of occurrence of the specific condition. In the ETC those percentiles are derived from model transmission spectra. Within the ETC, the user selected constraint determines which of several input files are loaded to define the sky transmission and emission and conditions the image size adopted for the nominal point source.

The CANARICAM ETC is available here:

http://gtc-phase2.gtc.iac.es:8080/itc/itc/servlets/ITCcanaricam.html

7 Forecasting the Precipitable Water Vapour above the observatories in the Canary Islands

Recently, with the collaboration of the Sky Quality Group at IAC (http://www.iac.es/proyecto/site-testing/), I have designed and developed a Precipitable Water Vapour (PWV) forecasting system based on a mesoscale numerical weather prediction model known as WRF (Weather Research and Forecasting). The system is named FOR-O (FORrecasting the Observatories) and is providing PWV forecasts for both ORM and OT (Observatorio del Teide) since october 2018. In this chapter I will expose such a system and the implications it may have in the queue mode (flexible scheduling) of observations at GTC the availability of a 72-hour forecast of PWV above the observatory.

The FOR-O system is available in the following website: http://vivaldi.ll.iac.es/proyecto/site-testing/index.php?option=com_content&task=view&id=124&Itemid=147

7.1 Basic description of the For-O system

The concept of Forecasting for the Observatories (For-O) arises from the need of an accurate forecasting of the Precipitable Water Vapor (PWV), which severely impacts observations at Infrared wavelengths, at the observatories managed by the Instituto de Astrofísica de Canarias (IAC): Observatorio del Roque de los Muchachos (ORM) and Observatorio del Teide (OT). Such forecasting has been implemented as a platform running a mesoscale Numerical Weather Prediction (NWP) model, the Weather Research and Forecasting (WRF) model (currently version 3.8 in the For-O operational system). This platform includes full monitoring of the WRF model execution and easy interaction with the user through a integrated web front-end.

ForO runs the WRF model four times a day (at 00, 06, 12 and 18 UTC) providing 72 hours forecasts for the PWV above ORM and OT, following the schedule shown in the next figure:

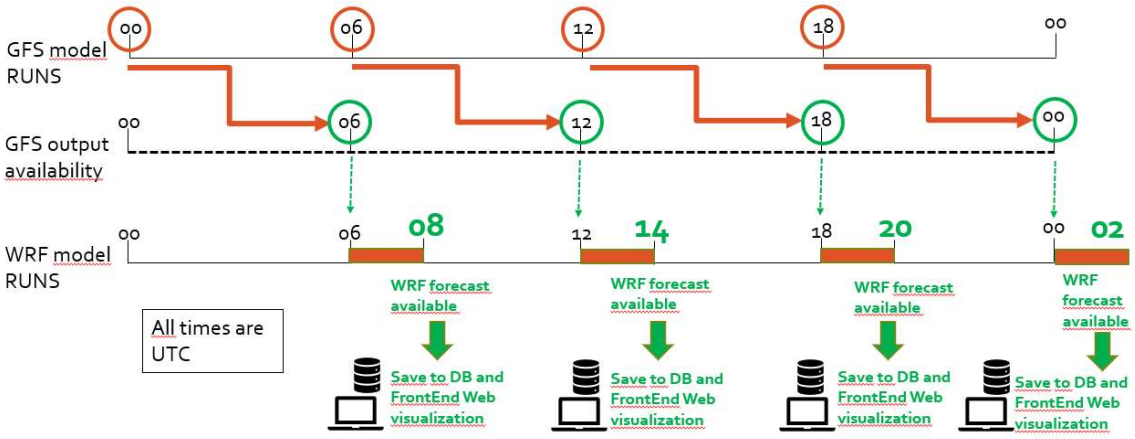

Fig 15. For-O system execution Flow in operational mode. The WRF model is run four times a day at 00, 06, 12 and 18 UTC following the availability of the GFS global model giving the initial and boundary conditions needed by WRF.

Independent WRF model runs are executed for each astronomical site to provide specific PWV forecasts above each observatory. The WRF model in ForO uses the output of the Global Forecasting System (GFS) global model as initial and boundary conditions every 3 hours through the whole forecasting range.

This system currently generates two final products:

1. PWV forecasts time series: 2 independent time series, for ORM and OT.
2. PWV forecast 2D charts: for the desired domains (d01 (27km), d02 (9km), d03 (3km)), centered at each observatory (ORM and OT).

While product 1 (PWV time series) shows the predicted PWV above the specific observatory, product 2 (PWV color plots) provides a 2D view of the PWV structure above the observatory height at synoptic scale for 3 different model domains at horizontal resolutions of 27, 9 and 3 kilometers, as shown in the following examples:

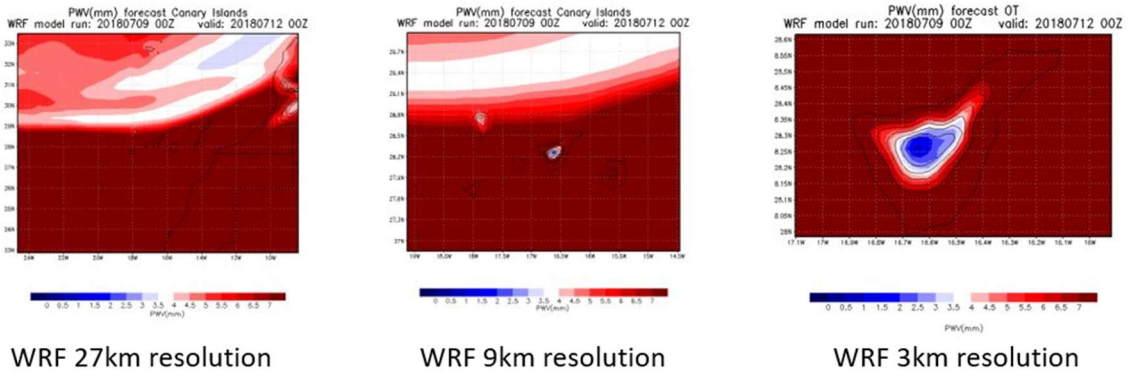

Fig 16. Examples of dynamical plots delivered by the For-O system. The PWV above the observatory height is plotted for each model domain at 27, 9 and 3km horizontal resolution.

This two final products are described in more detail in the following section. The WRF model is centered above each observatory coordinates, which are:

- For Observatorio del Roque de los Muchachos (ORM): 28.76° Latitude -17.88° Longitude
- For Observatorio del Teide (OT): 28.30° Latitude -16.51° Longitude

The raw output of the WRF model is automatically adjusted following the calibration described in Pérez-Jordán et al (2015) and Castro-Almazán et al (2016) for a model horizontal resolution of 3km, using high resolution radiosoundings. The PWV time series include the Total Forecast Error as described in full detail in Pérez-Jordán et al (2018). The detailed configuration of the WRF model implemented in ForO can also be found in this later publication.

Besides display of forecasted PWV above the observatories, the web interface allows the user to check the state of the current WRF run (if the model is running in that moment) or know the next scheduled time for WRF model run. Finally, a Download sections allows the user to get PWV historical data from the system in ASCII format up to 6 months (different options available in the drop-down menu).

7.2 Final products delivered by For-O

PWV FORECASTED TIME SERIES

The PWV forecasted time series show the predicted evolution of the PWV (y-axis, in mm) over time (x-axis, date and time UTC). The plot is divided by a vertical line, which indicates de latest WRF model run time (also marked in the plot with the label "Forecast Start", into two parts:

- To the left of the line is the latest 24 hours PWV as predicted by the WRF model in the latest 4 runs (shown in blue color). This "past forecast" can be used to make a verification of the forecasts with PWV observational data (for example, from the PWV monitor based on GPS in operation at ORM) or based on the infrared instrument performance used last night (for example: from the registered instrument sensitivities). In this sense, we have included also the latest PWV observations by the Water Vapour monitor based on GPS in operation at both ORM and OT (shown in green color).

- To the right of the vertical line is the next 3 day (72 hours) forecast of PWV above the observatory. An additional vertical line in green color shows the "Present time", which is automatically set every time the user access this plot. It helps the user to locate the present moment and its PWV forecasted value.

This is a hourly time series, so a total of 96 data points are shown. Together with predicted values for the PWV, also an error bar is displayed. This error bar reflects the Total Forecast Error and it is computed following Pérez-Jordán et al (2018). This total error takes into account the

degradation of the forecasts for longer forecast horizons and the instrumental uncertainties of the sensors used in the WRF model calibration. The superposed observed PWV time series from the GPS monitor is expected to be used as a qualitative aid for the user to assess whether the forecasted PWV from the model agrees with observations. It should be noted, however, that the GPS water vapour monitor has its own uncertainties (usually in the range 0.5 – 1mm PWV) and that the plotted values correspond to the ones available in real-time, which are a first estimation based on fixed GPS satellite orbits (known as the "rapid" value). This value is 48 hours later more accurately determined by the GPS monitor but it is not reflected in this plot.

An example of the time series plot is shown below:

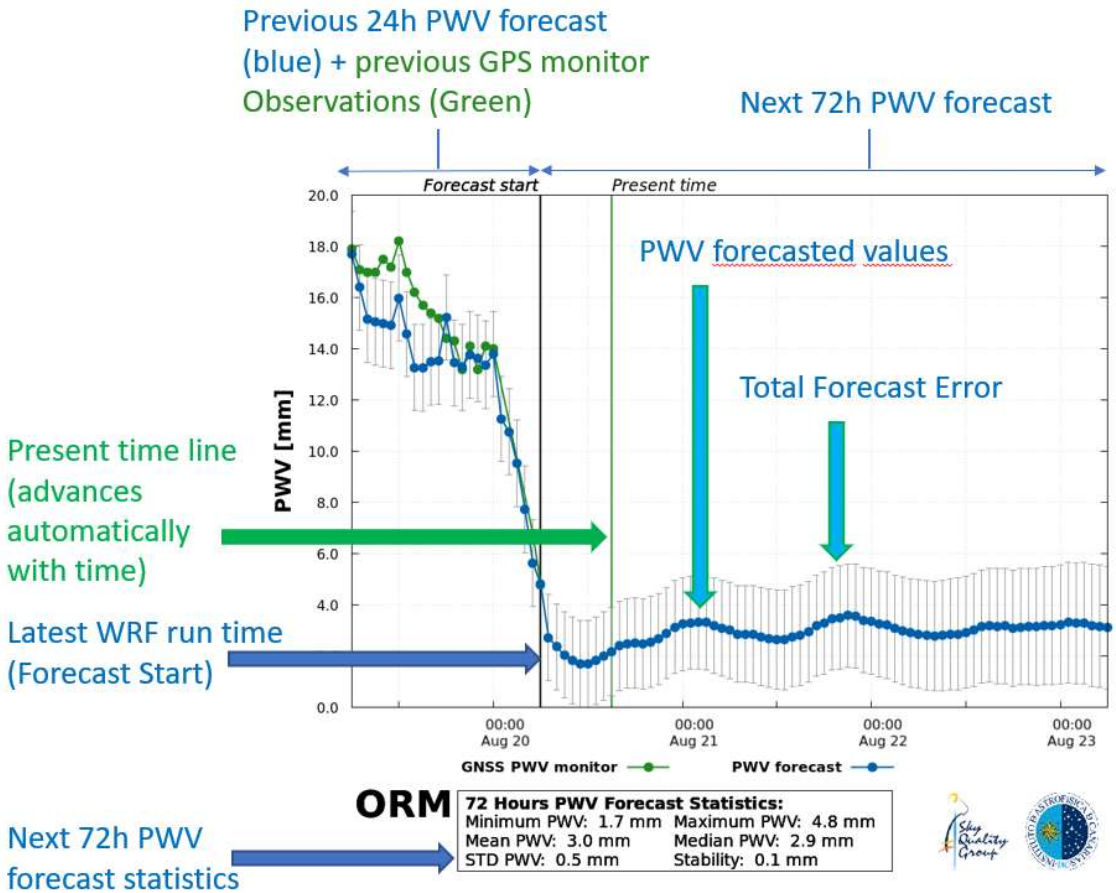

Figure 17. Example of the hourly forecasted PWV time series generated by For-O. Superposed in the plot is the “real-time” measured PWV by the GPS monitor in operation at ORM.

The time series plot allows user interaction by moving the mouse over any of the two time series plotted, the PWV forecast or the GNSS monitor PWV measurements, to easily read the PWV value and better compare the forecasted and measured PWV.

To compute the PWV, we integrate the water vapour mixing ratio in the vertical above the observatory (i.e: for Airmass=1) from the level corresponding to the long-term average atmospheric pressure and taking the closest model grid point at 3km horizontal resolution, as shown in the next figure 18, which is an example for the ORM:

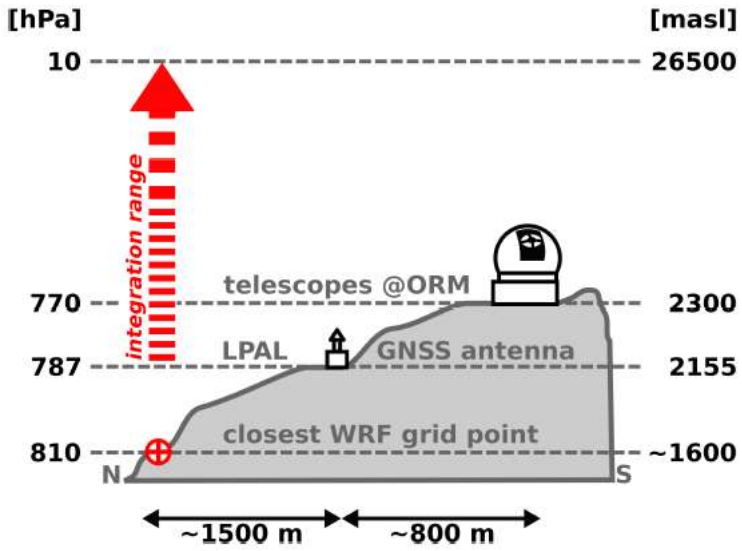

Figure 18. Procedure to derive the PWV above the GPS antenna pressure level up to 10 hPa by vertically integrating the water vapour mixing ratio. The WRF model grid point at 3km resolution is also depicted in the image to show the effect of the steep orography of the observatory.

To give a final value for the PWV forecasted value, specific calibrations for each observatory are applied following Pérez-Jordán et al (2015) and Castro-Almazán et al (2016). These calibration have been derived for the 3km horizontal resolution domain after a validation with high resolution radiosonde balloons at ORM and OT. As the main goal of the ForO system is to help astronomers to schedule infrared observations taking the most of the instruments working at those wavelengths, we also include a set of useful statistics of the 72-hr PWV forecasted in a box

just below the time series plot. This statistics include: the minimum and maximum PWV, the mean, median PWV, standard deviation and PWV Stability expected in the next 72 hours. The last two parameters are provided to give an idea of the fluctuation of the PWV signal. As noted in García-Lorenzo et al (2010), the temporal fluctuations of PWV drastically affect the schedule of an observing night at a telescope/observatory working in queue mode. Knowledge of the temporal stability of PWV is also critical in polarimetric observations, which require that the conditions are as stable as possible during the whole observing sequence.

To compute the Stability we used the Absolute Differences method described in García-Lorenzo et al (2010), for Δt of 1 hour:

$$f_{\mathrm{AD}}(\Delta t) = \langle |PWV(t+\Delta t) - PWV(t)| \rangle$$

As a practical rule, low values of the stability are preferred with values ≤0.1mm indicating a very stable PWV signal.

PWV 2D CHARTS

These animations show the 2D forecasted distribution and evolution for the next 72 hours of the Precipitable Water Vapor (PWV) above the observatory height. In ForO, the WRF model has been configured to run on three nested domains (d01, d02 and d03) centered in Observatorio del Roque de los Muchachos (ORM) and in Observatorio del Teide (OT) with horizontal resolutions of 27, 9 and 3km respectively. Details on the domain configurations can be seen in the following table (figure from Pérez-Jordán et al (2018)):

Domain	Δx (km)	Grid	Surface (km)	Surface (degrees)
D01	27	60×45	1620×1215	$14.7° \times 11°$
D02	9	52×40	468×360	$4.2° \times 3.3°$
D03	3	40×25	120×75	$11.1° \times 0.7°$

In these maps, the PWV has been computed integrating the water vapour mixing ratio from the long-term mean pressure level corresponding to the observatory height, up to 10 hPa. In the

Canary Islands the predominant presence of a temperature inversion caused by subsidence, helps to trap most of the water vapour below it maintaining relatively dry and transparent skies above. Atmospheric water vapor decreases steadily in the vertical and most of the time it is confined in the first kilometers above the surface. This is clearly seen in the following mean and median vertical profiles of the water vapour mixing ratio obtained with data from 100 atmospheric balloons launched from Güímar sounding station (WMO station 60018):

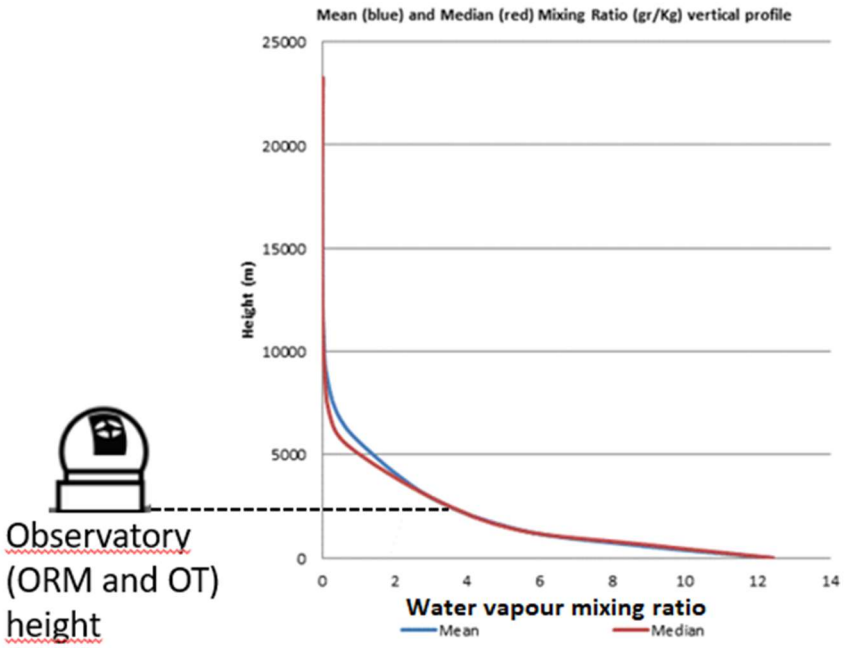

Fig 19. Mean and median vertical distribution of water vapour measured through the water vapour mixing ratio (in gr/Kg). These profiles have been obtained from 100 atmospheric sounding launched from the island of Tenerife.

Above the observatories (approximately 2400 m height) low levels of vapor mixing ratios are usually found. Some days, however, the subsidence inversion weakens or completely breaks down, allowing some water vapour to reach higher levels and thus increasing the PWV above summit. This is why ForO system provides this kind of plots, helping the user to trace future moist airmasses passing above the observatory thus compromising infrared observations. They also give a synoptic view of the PWV structure at different spatial scales.

The Grid Analysis and Display System (GrADS) has been used to automatically generate PWV 2D plots. The first animation corresponds to the most external model domain, covering the Canary islands, Madeira and part of northwestern Africa while the next 2 domains zoom into La Palma island. The animation is a movie of the forecasted evolution of the PWV above the observatory height in 3 hours time steps.

The color bar in this 2D plots has been configured to enhance the detail in the low (i.e: PWV < 4 mm) values of PWV. The color bar has been centered on the median for the ORM (PWV=3.9mm) obtained by García-Lorenzo et al (2010). "Cold" (blue) colors reflect a dry atmosphere above the observatory likely suitable for infrared observations, while “Warm” (red) colors reflect a moist atmosphere not so transparent at infrared wavelengths. Using this customized color bar, we can visualize a richer spatial structure of the PWV above the observatory, as shown in the following example for the ORM:

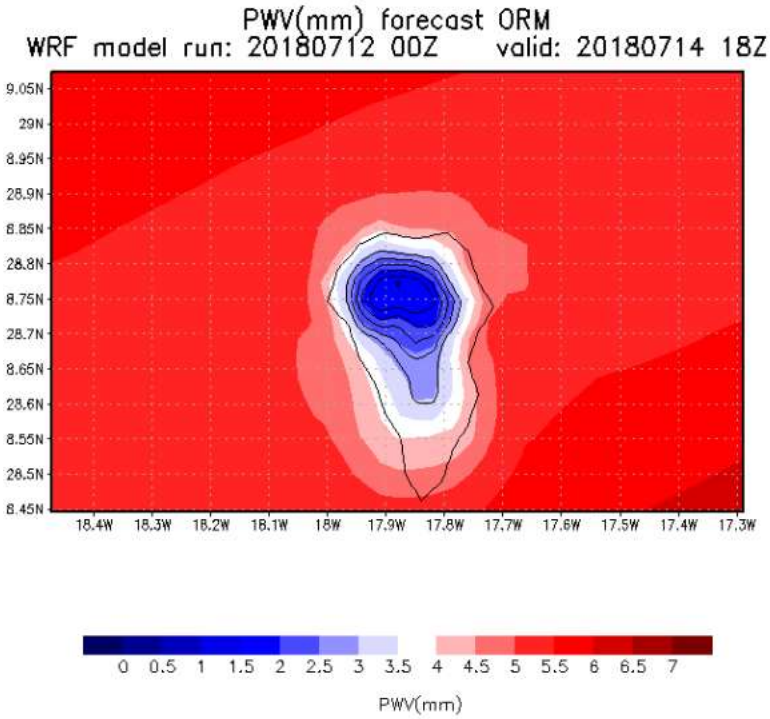

Fig 20. Example of a 2D PWV forecast chart for the innermost domain (the highest resolution one, d03) centered at ORM in La Palma island. The colour palette has been configured as to better show the spatial structure of PWV for low values of this variable.

8 Datasets and methods: PWV measured at ORM and CANARICAM observational data. Data analysis with the R statistical package.

In this work, we will use two datasets: the Precipitable Water Vapour (PWV) data measured by a GPS monitor located at ORM and the observing block (OB) data executed in Canaricam instrument at GTC. These two datasets will be described in detail in the following section. For the data analysis we have used R, an open source statistical language through the much user-friendly free tool called RStudio. The analysis method performed with R is also described in detail in the following chapter.

8.1 PWV data measured at ORM

The Precipitable Water Vapour (PWV) in the atmospheric column above the observatory has been routinely measured since 2008 at ORM using the GPS technique, which is based in the delays suffered by the GPS signal due to refraction of electromagnetic signals as they travel through the atmosphere. These delays are computed as the difference between the refracted and straight line optical paths after a least-square fit of the signals received from a number of GPS satellites (tipically 10) over a two hours averaging lag. The GPS station can measure the total delay, called the Tropospheric Zenith Delay (TZD) which in turn has two components: the Zenith Hidrostatic Delay (ZHD) which is very stable and related to the local atmospheric pressure while the other is related to local water vapour at the site (the wet delay or ZWD), and is more variable. In the determination of this Zenith Hidrostatic Delay, knowing the local pressure at the antenna location becomes very relevant to avoid systematic biases. This GPS antenna has a collocated Vaisala Barocap digital barometer (PTB330) which has a total accuracy of ±0.25 hPa. The Zenith Wet Delay is directly proportional to the PWV (in mm) through the following expression (Askne et al, 1987):

$$PWV = ZWD * \frac{10^6}{\rho R_v[\left(\frac{k_3}{T_m}\right) + k_2'} \; [mm]$$

Where ρ is the density of liquid water, R_v is the specific gas constant for water vapour and the refractivity constants $k_3$and k_2'have been determined empirically using microwave techniques (Bevis et al, 1994).

One of the main advantages of the GPS technique is that is has much better temporal resolution than radiosondes and might be almost continuously monitoring the PWV even in the presence of clouds. The GPS antenna is located in the roof of one of the ORM buildings near the Residence, exactly at latitude 28º45'49.9''N, longitude 17º53'37.8''W at an altitude of 2155 m a.s.l. The location and an image of the actual GPS antena is shown in figure 21. This GPS station is part of the international network (the International Association of Geodesy (IAG) Reference Frame Sub-Commission for Europe (EUREF)) of GPS stations.

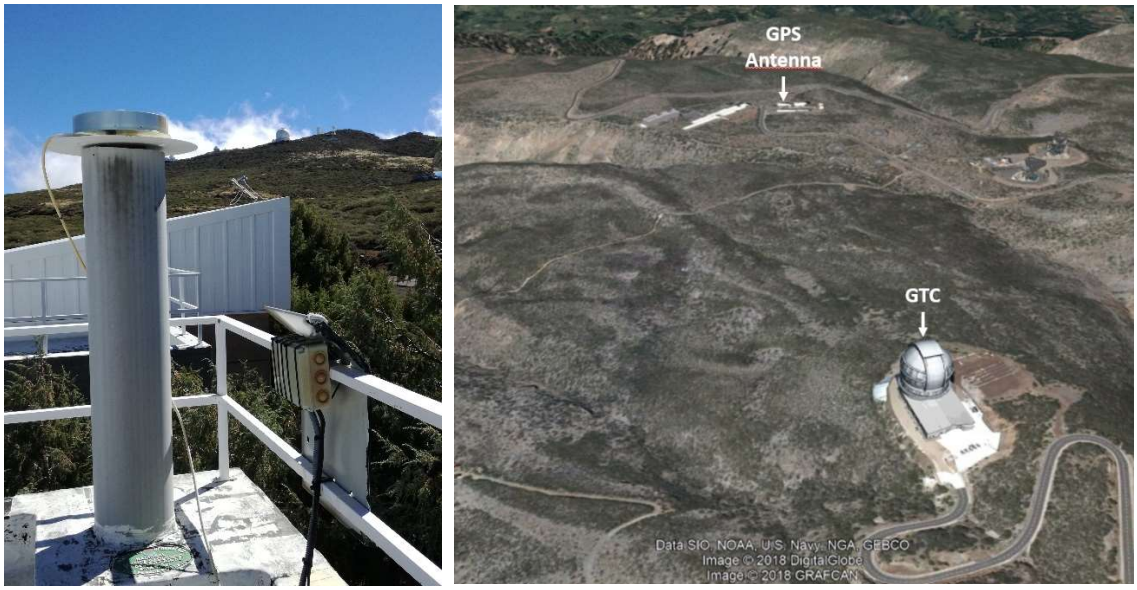

Figure 21. (left) The GPS antenna and its collocated barometer installed in the roof of the building which location is indicated in the Google Earth image (right) together with the Gran Telescopio Canarias (GTC) where the Canaricam instrument is hosted.

The dataset contains nearly 10 years of PWV measurements with a frequency of 30 min and we have selected only the night time PWV data, as is the one we are interested in, and has been calibrated to include the local pressure (collocated with the antenna). This dataset has been kindly provided by the Sky Quality Group at IAC.

8.2 CANARICAM observational data

The CANARICAM observation log has been kindly provided by the GTC (http://www.gtc.iac.es/). The observation log reflects executed Observational Blocks (or OB) with CANARICAM, from 2012-07-30 to 2016-03-16 (non consecutive nights) which are based on observation packages delivered to the PI (Principal Investigator). These OB's have been executed in queue mode of observations at GTC (explained in section 6.1). The CANARICAM log file has the following data fields: OB identifier, date (YYYY/MM/DD), maximum required PWV in milimeters (as specified by the PI), the night (support) astronomer judgement of whether this requirement was fullfilled or not and filters used in each OB. To verify this, the support astronomer has the real-time PWV measured by the GPS monitor described in the previous section, so it makes sense to make an analysis of both datasets and its relationships. The original file has 1027 rows (thus, OB's) which have been filtered and cross-analyzed with the PWV dataset using the R statistical package.

8.3 Data analysis with R statistical package

In R we will import the original datasets into a specific object in R called "dataframe", as it is a very flexible means of working with large data files structured in rows and columns. In the following, the detailed R instructions used in each step of the analysis is detailed and explained.

9 Analysis and Results: CANARICAM observation log and PWV measurements by GPS monitor. CANARICAM measured flux and sensitivity data. Discussion.

9.1 CANARICAM observation log and PWV time series in the same nights

The original datasets are named: PWVMo_ORM_3 (the PWV measurements from the GPS monitor) and CanaricamFull_2 (CANARICAM observation log). In the following, the PWV values used are the calibrated ones, which include a calibration with high resolution radiosoundings.

In order to better compare both datasets, the first thing we have done is to convert the calendar date to Julian Day (JD). The expression used for this conversion is the following (from Kartunnen et al, 2007):

$$JD = 367y - \frac{\left\{7\left[y + \frac{m+9}{12}\right]\right\}}{4} - \frac{3\left\{\left[\frac{y + \frac{m-9}{7}}{100}\right] + 1\right\}}{4} + \frac{275m}{9} + d + 1721029$$

where JD is the Julian Date at noon, y is the year (YYYY), m is the month and d is the day, and the division means an integer division, the decimal part thus has been truncated. In R this is performed with special function %/% (integer division).

Using the instruction CBIND we add a new column with the computed JD to the original PWV dataframe:

```
PWVMo_ORM_3=cbind(PWVMo_ORM_3,JD=(367*PWVMo_ORM_3$V1)-
(7*(PWVMo_ORM_3$V1+(PWVMo_ORM_3$V2+9)%/%12))%/%4-
(3*((PWVMo_ORM_3$V1+(PWVMo_ORM_3$V2-
9)%/%7)%/%100+1))%/%4+(275*PWVMo_ORM_3$V2)%/%9+PWVMo_ORM_3$V3+1721029)
```

In the CANARICAM log file we add a new column with the JD computed as described above:

```
CanaricamFull_2=cbind(CanaricamFull_2,JD=(367*CanaricamFull_2$V2)-
(7*(CanaricamFull_2$V2+(CanaricamFull_2$V3+9)%/%12))%/%4-
(3*((CanaricamFull_2$V2+(CanaricamFull_2$V3-
9)%/%7)%/%100+1))%/%4+(275*CanaricamFull_2$V3)%/%9+CanaricamFull_2$V4+1721029)
```

Now we make a slight adjustment in the JD of the PWV dataset, to derive a new JD1, with the purpose to have in the same Julian Day the time interval between dawn of the previous day to

dusk of the following day, which consitutes for us, only one night of observation (an astronomical night) and thus we seek to use a unique identifier for the night, JD1. This is done in the PWV file as the night measurements comprises for the last hours in one JD to the first hours in the new JD, while in the CANARICAM file is only one JD of observations. The expression used for this adjustment is the following:

$$JD1 = trunc\{[JD + (H_{PWV})/24] + 0.5\}$$

where H_{PWV} is the hour in the original PWV file (PWVMo_ORM_3) and trunc is the R function to take the integer part. We will work with integer JD's, no decimals are needed.

This JD1 in the PWV file is the same as JD in the CANARICAM log file. So we now add a new column only in the PWV file with this new JD1, with the next instruction in R:

```
PWVMo_ORM_3=cbind(PWVMo_ORM_3,JD1=trunc(PWVMo_ORM_3$JD+(PWVMo_ORM_3$
V4/24)-0.5))
```

Next step is to obtain, for each date (JD1) in the PWV file (PWMMo_ORM_3), the (night) mean PWV (in our case, the PWV value is variable V10), using the R function "aggregate":

```
PWVmean=aggregate(V10~JD1,data=PWVMo_ORM_3,FUN=mean,na.rm=TRUE)
```

The new dataframe created (PWVmean) has only 2 columns: The JD1 and the night mean PWV JD1. Now, we will use again the aggregate function to obtain the single nights observed with CANARICAM. This is because in the original CANARICAM log file (CanaricamFull_2), most of the nights contains multiple Observational Blocks (OB), that is, multiple rows for each JD:

```
nightscanaricam=aggregate(V6~JD,data=CanaricamFull_2,FUN=mean,na.rm=TRUE)
```

So now we have a dataframe (nightscanaricam) with 2 columns: the JD and the night mean PWV requested by the PI. That is 222 nights observed with Canaricam.

Again, we use aggregate to obtain the total number of OB's executed with CANARICAM in each night:

```
obscanaricam=aggregate(V1~JD,data=CanaricamFull_2,FUN=NROW)
```

This is stored in a need dataframe we call “obscanaricam”. There were four nights in which the was no PWV data from the GPS monitor (NA values), so we filter them out and save it the “nightscanaricam2” dataframe:

```
nightscanaricam2=na.omit(nightscanaricam)
```

so we have a total of 218 nights useful for the analysis.

9.2 Determination of PWV_{Max}

First of all we will compute the number of nights in which the mean PWV measured by the GPS monitor (variable var3) was less or equal than the PWV requested by the PI (variable V6), in which case we will set "1" in a new column called"pwvok". Otherwise we will set “0" in this “pwvok” field:

```
nightscanaricam2$pwvok[nightscanaricam2$V6>=nightscanaricam2$var3]<-1
nightscanaricam2$pwvok[nightscanaricam2$V6<nightscanaricam2$var3]<-0
```

We obtain the following night count for each case:

```
sum(nightscanaricam2$pwvok==0)
```

[1] 57

> sum(nightscanaricam2$pwvok==1)

[1] 161

That is, in a (161/218)*100= 73.85% of the nights the condition for the required PWV was fulfilled, while in a in a (57/218)*100= 26.15% of the nights it was not.

Now we will filter, from the total 218 nights observed with CANARICAM and with valid and calibrated PWV measurements from the GPS monitor, those in which the PWV required (sky transparency constraint) was fulfilled. To obtain this value, we will generate a new column called "mask" which will be the result of the product of the PWV values measured by the GPS (var3) and the column "pwvok", derived in the previous step:

```
nightscanaricam2=cbind(nightscanaricam2,
mask=nightscanaricam2$var3*nightscanaricam2$pwvok)
```

Finally we define a new dataframe called "nightscanaricam3" with only those nights with CANARICAM observations in which mask≠0, that is, the nights in which the PWV constraint set by the PI was achieved, resulting in 161 nights:

```
nightscanaricam3=nightscanaricam2[nightscanaricam2$mask!=0,]
```

The column "mask" contains the PWV values measured by the GPS monitor in those nights.

We will use this dataframe to study more in detail its distribution, as this is the one which interest us. We will first plot the histogram of the variable "mask" with the density function superposed. To do so we will use the package easyGgplot2, which requires to install (and load it from the library) first devtools:

```
install.packages("devtools")

library(devtools)
```

we now download and install easyGgplot2 from Github:

```
install_github("kassambara/easyGgplot2")

library(easyGgplot2)
```

We plot the histogram with a bin width of 0.5mm, using the following command:

```
ggplot2.histogram(data=nightscanaricam3$mask,xName='PWV',binwidth=0.5, fill="white",
color="black",addDensityCurve = TRUE)
```

which is presented in figure 22, which includes also a inset with the main statistics of this distribution. We see that the PWV distribution is approximately Gaussian-like, or more exactly are three Gaussian distributions, one with the main peak at PWV≈1.7 mm, a secondary peak is at PWV≈5 mm and a third at PWV≈7.5 mm. 90% of the total PWV measured values during the nights observing with CANARICAM in which the PWV constraint was fulfilled, where below 6.3 mm. During each observing block (OB), more than one filter can be used, so for the total of 161 nights, we found 317 observations made with different filters. From this total observations, we see that about 65% were done with imaging filters in the 10 μm region (N band) and 27% with spectroscopy filters (gratings) also in the the 10 μm region (Lowres10), that give a total of ≈92% of observations with filters and gratings in the 10 μm. Given the shape of the density probability and that the main peak concentrates most of the sample population, we hypothesize that the obtained percentile 90 could be used as a practical threshold for CANARICAM (PWV_{MAX}), at least for observations with filters in the N band, that is, all silicate filters (Si1, Si2, Si3, Si4, Si5, Si6, SiC), the broad-band N-10.36 and the various narrow-band filters at these wavelengths (PAH1, PAH2, ArIII, SIV, NeII and NeII-ref2). The obtained value for PWV_{MAX} seems to be also in

agreement with the classification of infrared observing conditions as a function of PWV proposed by Kidger et al (1998), which was established as follows: 1) Good or excellent → PWV ≤ 3 mm; 2) Fair or mediocre → 3 < PWV ≤ 6 mm; 3) Poor → 6 < PWV ≤ 10 mm; and (4) Extremely poor → PWV > 10 mm. They established the frontier between fair and poor conditions in 6 mm of PWV, close to our threshold.

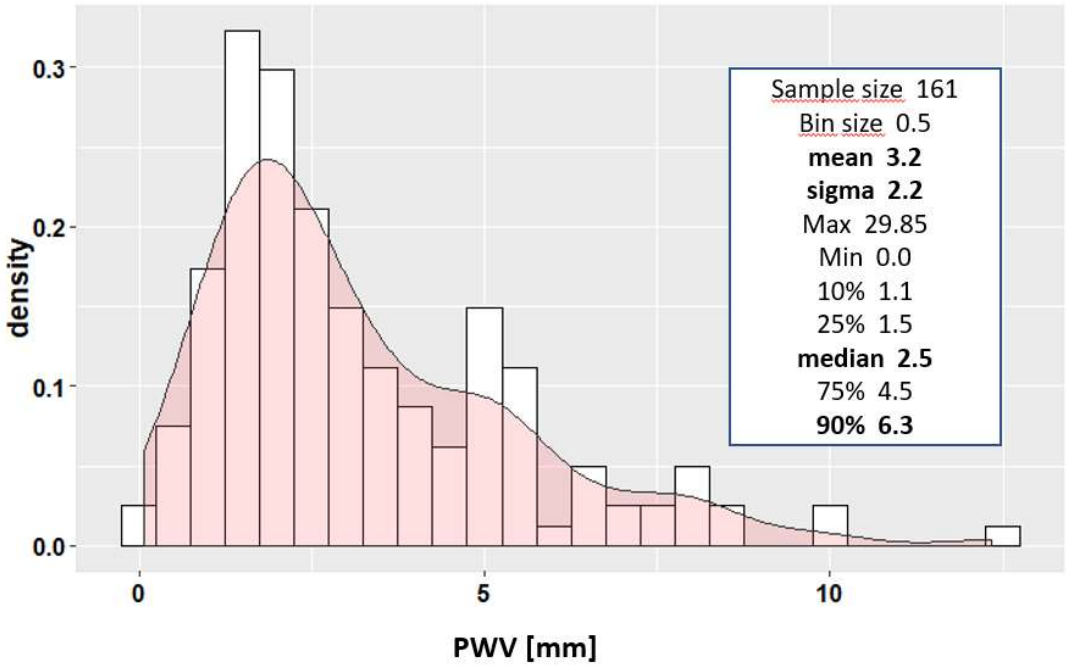

Figure 22. Histogram and density probability function for all the nights of observations with CANARICAM in which the PWV requirement was met. This distribution contains observations made with many CANARICAM filters working at diferent central frequencies. See the discussion in the text for more details.

9.3 Determination of $P_{PWV_{Max}}$ from PWV climatological data

A very extensive statistical study on PWV above ORM has been carried out previously based on data from a GPS receiver and a well established technique which allows to compute the PWV from the delays of radio waves as they travel across the Earth's atmosphere from the GPS satellites to the ground station (Garcia Lorenzo et al, 2010). The data sample in these

aforementioned work consisted of 31500 individual estimations of the PWV with a temporal resolution of 2 hours, covering ~ 7.5 years (from June 2001 to december 2008). The PWV above ORM shown a well defined seasonal behaviour, being winter and spring the best seasons in terms of PWV, with lowest mean and dispersion (σ) values of PWV. More than 60% of the nights during February, March and April had measured values of PWV ≤ 3 mm. One of the main conclusions of Garcia Lorenzo et al (2010) is that ORM is a very good site for IR observations when is compared with a site at a significant higher altitude as Mauna Kea, which is located more tan 1300 meters higher. Based on the PWV data obtained from GPS stations at both sites they determined that for each 10 hours of good IR conditions (PWV ≤ 3 mm) at Mauna Kea, we have 6 hours at ORM with the same conditions, using the total data sample. When using only the winter and spring subset, these figures increase to 7.9 and 7.4 hours respectively with PWV ≤ 3 mm at ORM for each 10 hours at Mauna Kea.

In this work we will use the updated climatology sample of PWV measured by the GPS monitor from 2008 to 2017, so that accounting for almost 10 yr of continuous PWV monitoring at ORM. This new dataset has a higher temporal resolution of 30 min. From this data we have selected only night time PWV values from 2008/07/01 to 2017/06/30 and its global statistics are resumed in the following table:

N	Mean	Median	σ	P10	P25	P75	P90	Max	Min
25819	4.97	3.90	3.89	1.2	2.1	6.8	10.22	29.8	0

where N is the sample size (only night-time PWV measurements, taken with a frequency of 30 min), and the mean, median, standard deviation (σ), the percentiles and maximum and mínimum are all expressed in mm.

In figure 23 we have plotted the relative frequency distribution along with the probability density function. In this case, the density function is clearly Gaussian-like, with its peak at low PWV values around 2 mm and with a long tail which reflects the high variability of PWV.

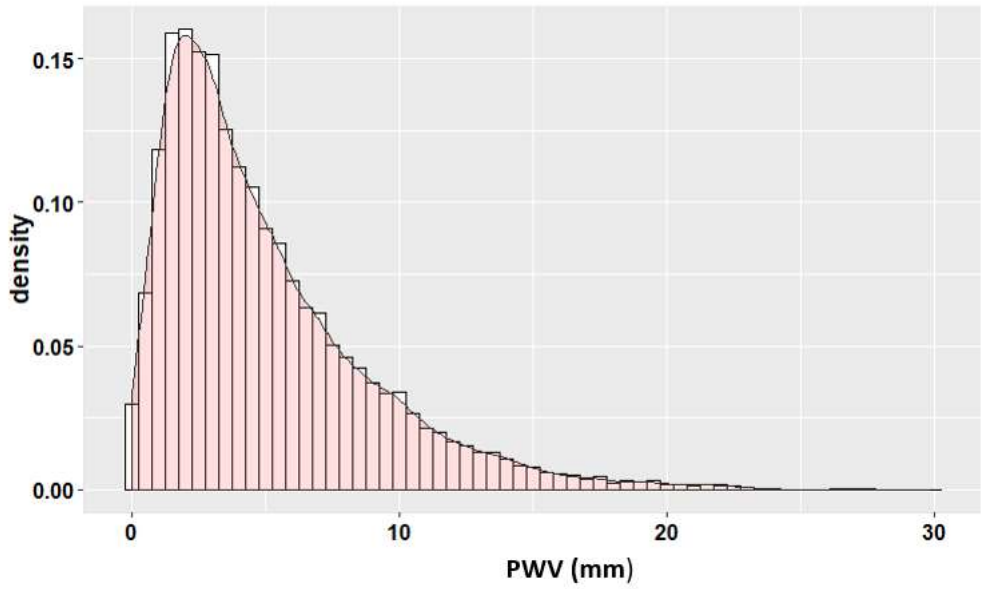

Figure 23. Relative frequency histogram with the superposed probability density function of the night time PWV measured by the GPS monitor at ORM, covering ≈10 yr. The bin size has been configured to 0.5 mm.

We will use now this distribution of night time PWV at ORM (≈10 yr, N=25819 observations), setting the previously obtained PWV threshold, $PWV_{MAX} = 6.3\ mm$ we obtain the probability of having the PWV below this threshold, $P_{PW\ \ MAX}$, which is 72%.

9.4 Sensitivity measurements with CANARICAM at GTC: estimating sensitivity from PWV

In this chapter we use CANARICAM sensitivity measurements published in the GTC website during four nights in 2012 and 2013 and match this measurements with PWV data available from the GPS monitor. The exact dates, the standard stars used for the measurements and the PWV night statistics from the GPS monitor (mean, median and sigma) are summarized in the next table:

Date	Standard Star	Night mean PWV	Night median PWV	Night σ PWV
03/03/2012	HD70272	1.96	2.01	0.32
05/06/2012	HD96833	5.54	5.47	0.74
29/01/2013	HD3712	2.88	2.85	0.28
18/08/2013	Hd3712	9.72	9.84	1.38

The following scatter plots and linear regressions have been computed using the Sensitivity measured at 4 dates during commissioning (nights of 2012/03/03 and 2012/06/05) and testing of CANARICAM (nights of 2013/01/29 and 2013/08/18). These data are available at the GTC website:

http://gtc.iac.es/instruments/canaricam/data-commissioning.php

http://gtc.iac.es/instruments/canaricam/canaricam.php

In figure 24 we plot the measured sensitivity (in mJy) as a function of the central wavelength for all the CANARICAM filters, broadband and narrowband, for both bands N and Q. Here the following definition of sensitivity is used: the sensitivity in CANARICAM is measured as the flux of a source yielding a SNR (Signal to Noise Ratio) of 5 in 1800 sec on-source time using aperture photometry, thus the smaller the sensitivity value, the more sensitive is the instrument (which can detect sources yielding weaker fluxes). The aperture radii used is the one giving the maximum SNR.

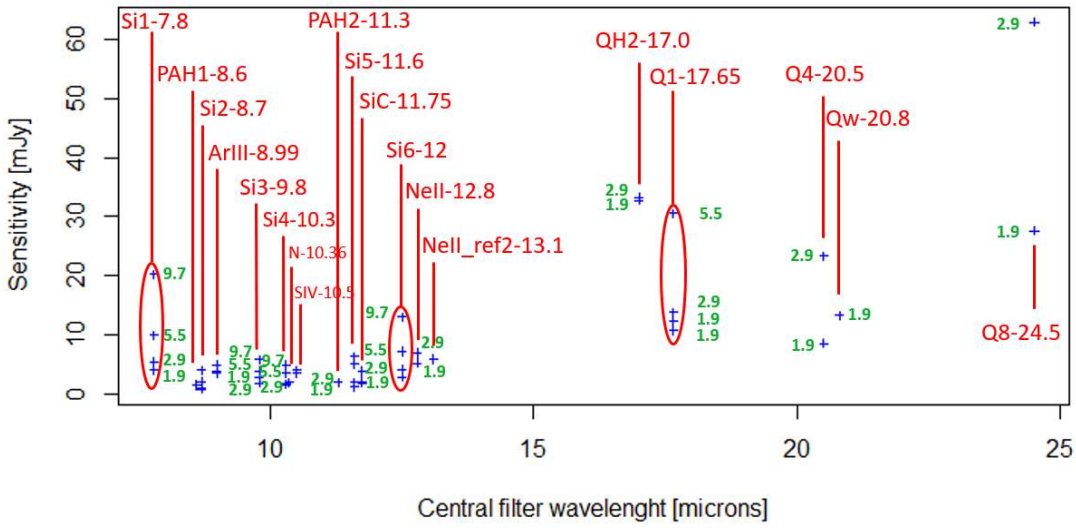

Fig 24. CANARICAM estimated sensitivity (in mJy) for a 5-σ detection in a 30-min on-source time as a function of wavelenght and night mean measured PWV. Data points are stacked up at each filter central wavelenght, as indicated in the figure in red text (filter name and central wavelength). For a certain filter, the sensitivity values in the vertical correspond to different dates with different PWV measured by the GPS monitor (PWV values in milimeters in green colour), with higher values of sensitivity (thus, poorer) at higher PWV. For the sake of clarity, the PWV has been included only for certain points. See the discussion of this figure in the text for further details.

From this plot we can identify the filters which are severely impacted by the increase of PWV, and have been marked with and ellipse. We can also see the severe effect of even low amount of PWV can have in the instrument sensitivity when operating at longer wavelenghts in the Q band: an increase of 1 mm in PWV represents a degradation in the sensitivity by a factor of more than 2 in the Q8 filter and close to 3 in the Q4 filter.

From this observed behaviour for the total sample of 4 nights, we will focus on the four more affected CANARICAM filters and the ones with more sensitivity measurements (Si1, Si6 and Q1) and find its linear regression and least square fit. Figures 25, 26 and 27 show the scatterplots corresponding to the Si1, Si6 and Q1 CANARICAM filters, respectively.

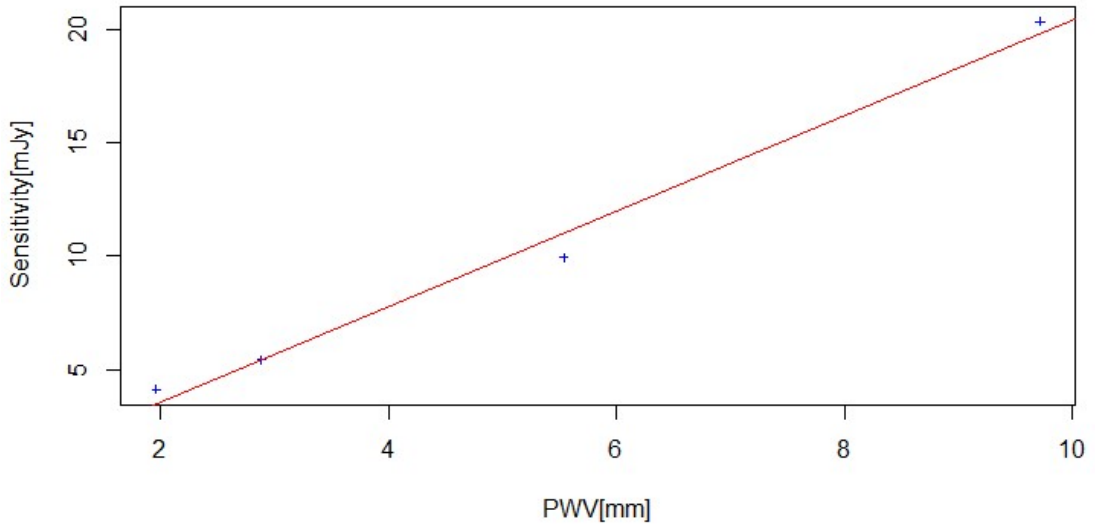

Fig 25. Scatter plot showing the linear relationship between the CANARICAM measured sensitivity (in mJy) and the measured Precipitable Water Vapour (PWV) by the GPS monitor, for the Si1 (7.8 μm) filter.

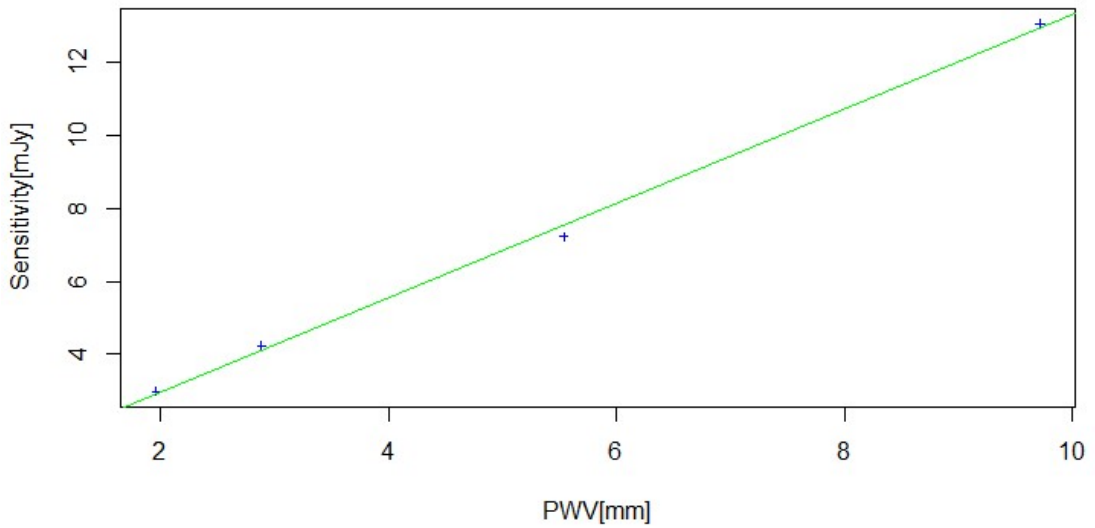

Fig 26. Same as Fig.25 but for the Si6 (12.5 μm) filter.

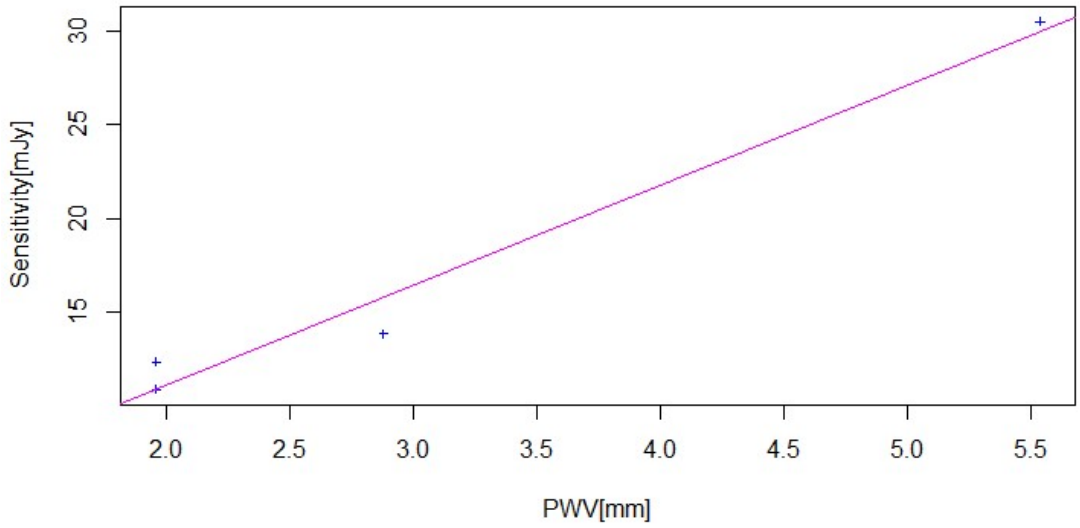

Fig 27. Same as Fig.25 but for the Q1 (17.65 μm) filter.

From the least square fit we obtain the following set of equations, where S is the expected CANARICAM sensitivity (in mJy), as defined previously, for the indicated filter and PWV (in mm) is the measured Precipitable Water Vapour from the operational GPS monitor, or the PWV forecasted values from the FOR-O forecasting system for the ORM:

Filter Si1: $S_{Si1} = 2.1018 * PWV - 0.6117$

Filter Si6: $S_{Si6} = 1.2867 * PWV + 0.4042$

Filter Q1: $S_{Q1} = 5.3446 * PWV + 0.3895$

From these results we see that the measured sensitivity and PWV are highly correlated. These equations allow the astronomer to have an estimation of the expected sensitivity of the CANARICAM instrument as a function of the present PWV conditions.

In those dates the PWV measured by the GPS monitor suffered of important systematic biases due to the unavailability of local pressure measurements (side by side with the GPS antenna). The in-situ accurate measure of pressure is critical in computing the PWV as explained before in section 8.1. Our analysis and derived equations for computing the CANARICAM sensitivity as a fuction of PWV are corrected of the aforementioned biases as we used the latest PWV dataset which incorporates the local pressure data.

We are now going to extend these results to the rest of Silicate filters (Si2, Si3, Si4, Si5) as these filters are the most often used in CANARICAM and also because we still have at least the same or more number of sensitivity measurements as with Si1 and Si6. The scatter plots for these filters are shown in figures 28 to 31.

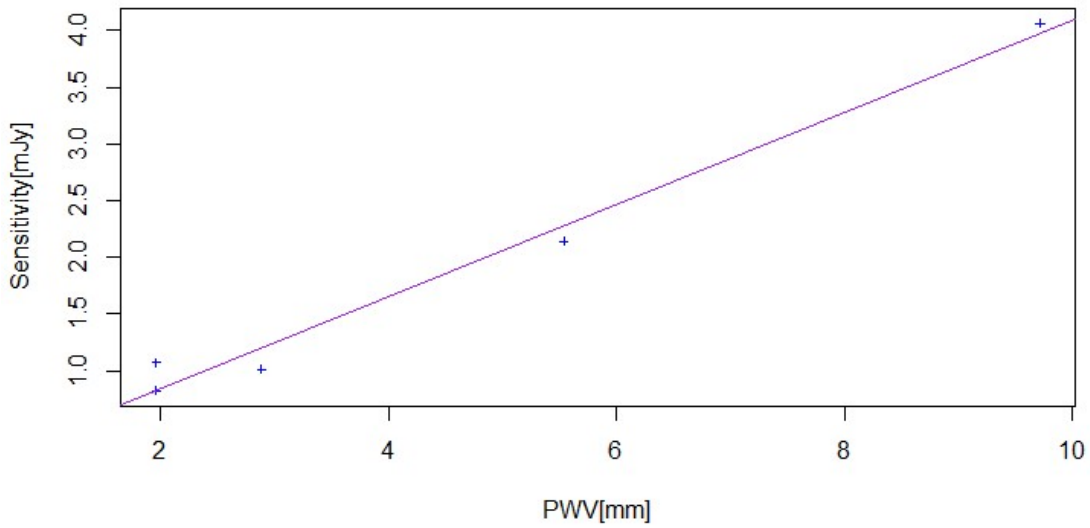

Fig 28. Scatter plot showing the linear relationship between the CANARICAM measured sensitivity (in mJy) and the measured Precipitable Water Vapour (PWV) by the GPS monitor, for the Si2 (8.7 µm) filter.

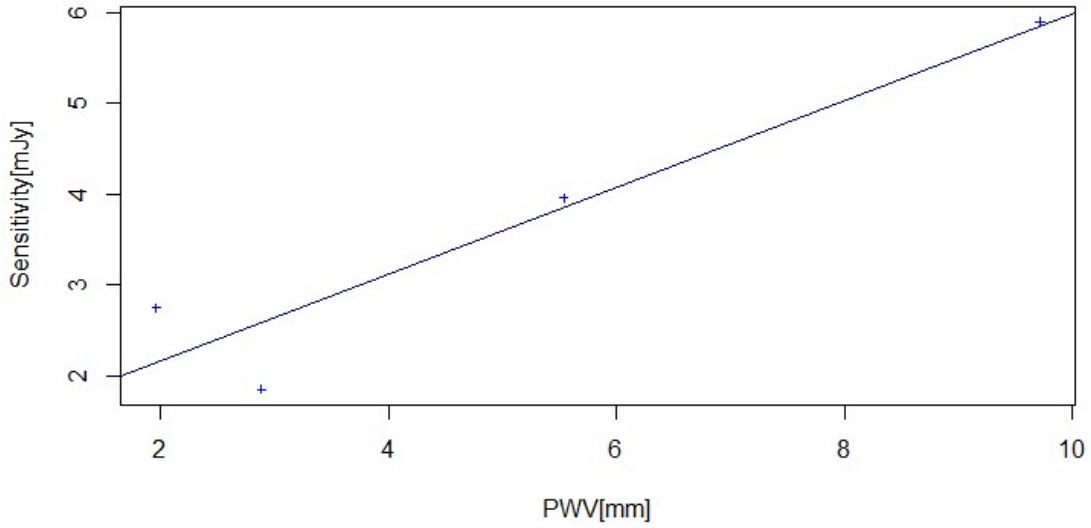

Fig 29. Same as Fig.28 but for the Si3 (9.8 µm) filter.

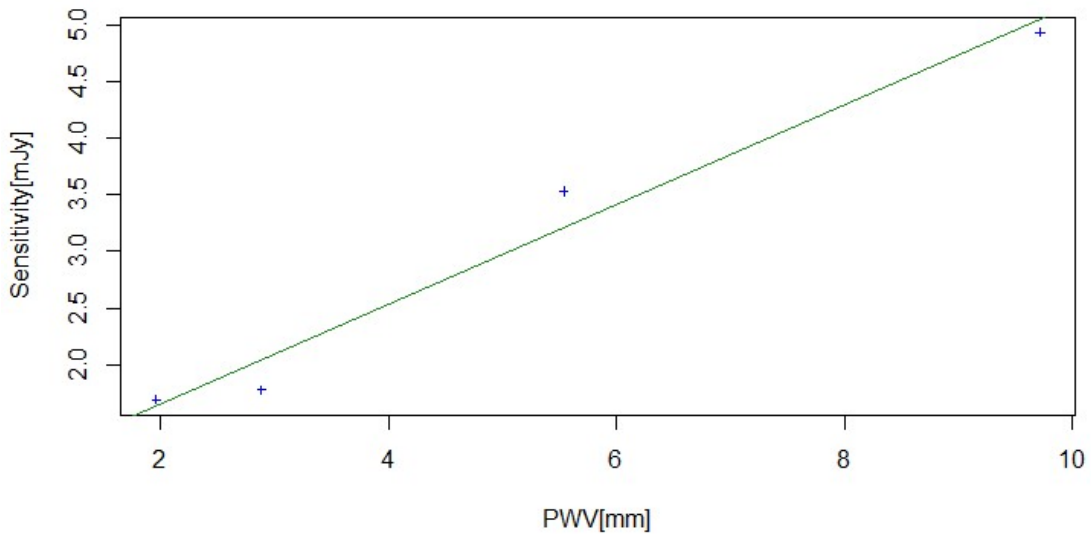

Fig 30. Same as Fig.28 but for the Si4 (10.3 µm) filter.

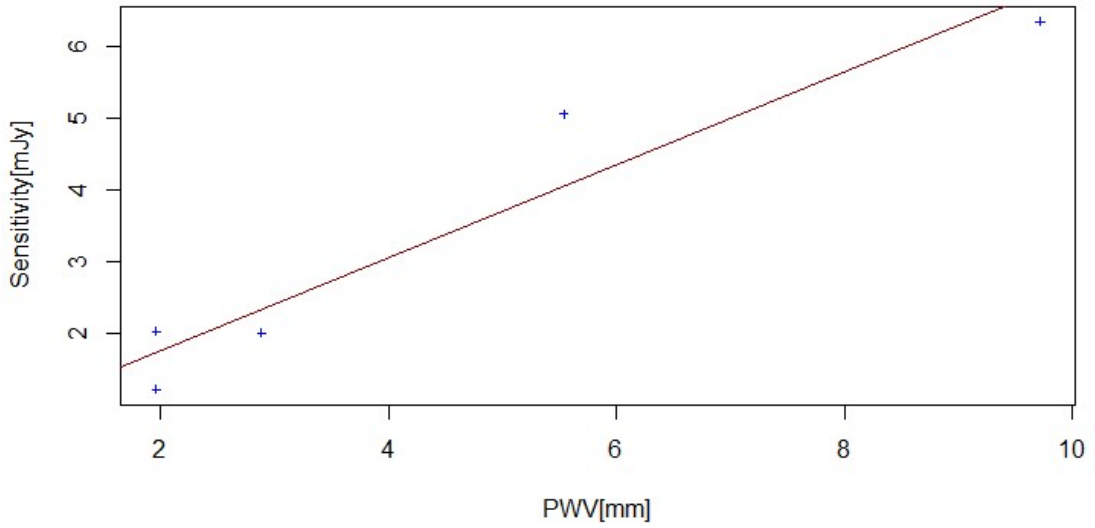

Fig 31. Same as Fig.28 but for the Si5 (11.6 µm) filter.

The resulting regression equations are the following:

Filter Si2: $S_{Si2} = 0.4058 * PWV + 0.0295$

Filter Si3: $S_{Si3} = 0.4777 * PWV + 1.2145$

Filter Si4: $S_{Si4} = 0.4398 * PWV + 0.7725$

Filter Si5: $S_{Si5} = 0.6473 * PWV + 0.4780$

A summary of the regressions results for all analyzed filters is shown in the next table:

Filter	N	R^2	Intercept	Slope
Si1	4	0.989	0.6117	2.1018
Si2	5	0.983	0.0295	0.4058
Si3	4	0.900	1.2145	0.4777
Si4	4	0.974	0.7725	0.4398
Si5	5	0.918	0.478	0.6473
Si6	4	0.997	0.4042	1.2867
Q1	4	0.975	0.3895	5.3446

For all filters, the determination coefficient (R^2) is ≥ 0.900. Of course, the sample size is small due to the few sensitivity measurements available. It is proposed as future work in the next section to obtain further measurements in those filters with as many PWV conditions as posible, to obtain more accurate regression equations based on the least square linear fits.

9.5 Hypothesis test case using CANARICAM data published in the literature.

In this section we use available data in a published paper which used data from Canaricam observations, and the 2 datasets used in previous sections: the Canaricam OB log file and PWV measured by the GPS monitor at ORM, to test the previous hypothesis regarding a practical threshold for the maximum PWV which would allow observing with Canaricam. Based on the dates of observation indicated in the paper and the used filters we could identify the exact OB's assigned to this project and also match these data with the PWV measurements from the GPS monitor.

Observations of the Lensed Quasar Q2237+0305 with CanariCam at GTC

In this paper (Vives-Arias et al, 2016) the authors present new mid-IR observations of the quadruply lensed quasar Q2237+0305 taken with Canaricam on the Gran Telescopio Canarias. In section 2 of their paper they describe the GTC observations with Canaricam of Q2237+0305 in 2012 July and 2013 September. The 2012 july observations were discarded because a non-Gaussian horizontal noise pattern appeared in the images that difficults the accurate measurement of fluxes of targets with low signal-to-noise ratios. The exposure times were increased for the last set of observations performed in 2013, using the same configuration to obtain three images on September 18 and two on September 19 with total on-source exposure

times of 3 x 1853.3 and 2 x 1522.4 s, respectively. With these new exposure times the target was succesfully detected and a final combined image was obtained using only the 2013 observations due to their better instrumental conditions, but the third image from September 18 was excluded, because of its very poor SNR due to a significant rise in the PWV, as indicated in the paper. Three images were obtained the night of 2013/09/18 and this project had 5 OB's assigned that night, which had PWV values in the 5.4 – 7.6 mm range. From the PWV dataset measured with the GPS monitor, we can see that the larger values took place in the first half of the night. Assuming a sequential order in the OB execution in the order reflected in the Canaricam log file and an approximate length of 1 hour for each OB, the first 3 OB's for this project were executed with PWV in the 6.5-7.6 mm range, while the other 2 with PWV in the 5.5 – 6.4 mm, so it is likely that the discarded image was taken during the first OB's with higher PWV values (in the paper they indicate a steep rise in PWV which seems to correspond to the first half of the night). The 2 images obtained in the following night (2013/09/19), where 2 OB's were assigned to this project, one in the beginning and the other by the end of the night, were executed with PWV values in the 1.9 – 4 mm range. That night the target was detected and both images obtained were succesfully used to combine for the final image, even though the exposure times were shorter that in the previous night. The following table shows a summary of all the relevant data from these 2 nights of observations, including PWV statistics derived from the GPS monitor:

Date	Filter	#OB	Exposure (sec)	mean PWV	median PWV	σ PWV	max PWV	min PWV
18/09/2013	Si5-11.6	5	3 x 1853.3	6.65	6.6	0.7	7.6	5.4
19/09/2013	Si5-11.6	2	2 x 1522.4	3.16	3.3	0.68	4	1.9

This result suggest an agreement with the previously obtained $PWV_{MAX} = 6.3\ mm$ which would allow observations with Canaricam (section 9.2), as in the first night, with PWV mean and median values ≈ 6.6 mm and values in the [5.4 – 7.6] mm range, one of the three images obtained with CANARICAM had to be discarded due to bad SNR while the second night, with PWV mean and median values ≈ 3.2 mm and values in the [1.9 – 4] mm range both images obtained with CANARICAM were succesfull.

10 Summary and conclusions. Proposed criteria for IR observations with CANARICAM. Future work.

Based on the obtained results, we can summarize the main findings as follows:

- We find that a unique PWV threshold for observation with CANARICAM cannot be established, as it depends on various factors, being the observation band (thus, the filter used) and the specific source under observation the most relevant. Nevertheless, a operative threshold for observations with CANARICAM which could be used at least with the most common filters (Silicate medium-band around 10 µm and Lowres spectroscopy grating also around 10 µm) has been determined from the density function of the CANARICAM observations dataset together with the PWV data measured at ORM with operational GPS monitor. This threshold has been determined to be $PWV_{MAX} = 6.3\ mm$.
- We found at least one reference in the literature in which real observations with CANARICAM for a specific science program would confirm the proposed PWV threshold of 6.3 mm. During a observing night with mean PWV of 6.65mm (as measured by the GPS monitor) one of the three images had to be discarded due too poor SNR.
- Once we have determined this practical threshold (PWV_{MAX}), we have determined from the climatological PWV data (≈10 yr) the probability of having the PWV below this threshold, $P_{PW\ \ MAX}$= 72%. So one can expect that 72% of the time, observations with CANARICAM are feasible at least in the N band.
- From the CANARICAM sensitivity measurements made during commissioning and test phases with CANARICAM, we have found the dependence of the instrument sensitivity on PWV but also on the filter, being some filters much more sensible to the increase of PWV than others.
- From the sensitivity measurements we have derived linear relationships that allow to estimate the instrument sensitivity (in mJy) once one knows the PWV amount above the observatory, which can be obtained in real-time from the PWV GPS monitor or, if one wants to schedule observations depending on the PWV conditions expected for the next (up to 72) hours, from the FOR-O PWV forecasting system in operation. This relationships can be useful for the PI when he/she needs to fill in the observation request the PWV requirement, and also for the support astronomer, when doing flexible

(service) mode of observations, which are programmed as the weather conditions change, deciding which project adjust better to the prevailing PWV conditions as he/she knows the filters needed for each science project.

The linear relationships obtained from sensitivity measurements can be improved, as the sample size for each filter was scarce, we propose to the GTC team the following:

- Use the common tasks to be performed during observations with CANARICAM (e.g: calibrations with standard stars, photometric or spectro-photometric standards, etc) to measure also the sensitivity in order to have a much more rich sample and thus obtain a more accurate linear regressions and relationships for all CANARICAM filters.
- This could be implemented first for the most commonly used filters in CANARICAM, the silicate filters for imaging in the 10 µm spectral region, and then on a second phase extend it to the 20 µm band.

11 References

American Meteorological Society (AMS), Glossary of Meteorology, 2nd ed., Boston, Mass, 2000

Askne, J. and Nordius, H., Estimation of tropospheric delay for microwaves from surface weather data, Radio Science 22, 379-386 (June 1987)

Bevis, M., Businger, S., Chiswell, S., Herring, T. A., Anthes, R. A., Rocken, C., & Ware, R. H. 1994, Journal of Applied Meteorology, 33, 379

Dorta-Antequera P. Las inversiones térmicas en Canarias, Investigaciones Geográficas 15, 109-124 (1996). http://rua.ua.es/dspace/handle/10045/461

García-Lorenzo B., Eff-Darwich A., Castro-Almazán J., Pinilla-Alonso N., Muñoz-Tuñón C., Rodríguez-Espinosa J. M., 2010, MNRAS, 405, 2683

Castro-Almazán J. A., Muñoz-Tuñón C., García-Lorenzo B., Pérez-Jordán G., Varela A. M., Romero I., 2016, in Observatory Operations: Strategies, Processes, and Systems VI. p.99100P, doi:10.1117/12.2232646

Glass I.S, Handbook of infrared astronomy, Cambridge University Press, 1999

Hammersley P.L., Infrared quality of the Canarian skies, New Astronomy Reviews 42, 533-536 (Nov.1998).

Hartmann D.L., Global Physical Climatology, International Geophysics Series vol.56, Academic Press 1994

Kartunnen H, Fundamental Astronomy. Springer, 2007.

Kidger, M. R., Rodríguez-Espinosa, J. M., del Rosario, J. C., & Trancho, G. 1998, New Astronomy Review, 42, 537

Lockwood D.J. (2015) Rayleigh and Mie Scattering. In: Luo R. (eds) Encyclopedia of Color Science and Technology. Springer, Berlin, Heidelberg

Mason R, Wong A, Geballe T, Volk K, Hayward T, Dillman M, Ficher S and Radomsky J, “Observing conditions and mid-IR data quality” in [Observatory Operations: Strategies, Processes, and Systems II], Proceedings of the SPIE 7016, 70161Y (July 2008).

Muñoz–Tuñón C., Vernin J., and Varela A.M, Night-time image quality at Roque de los Muchachos Observatory Astron. Astrophys. Suppl. Ser. 125, 183-193 (1997)

Otárola A., Travouillon T., Schöck M., Els S., Riddle R., and Skidmore W., Thirty meter telescope site testing x: precipitable water vapor, PASP 122(890), 470-484 (2010).

Pérez-Jordán G., Castro-Almazán J.A., Muñoz-Tuñón C.. Precipitable water vapour forecasting: a tool for optimizing IR observations at Roque de los Muchachos Observatory, Monthly Notices of the Royal Astronomical Society, Volume 477, Issue 4, 11 July 2018, Pages 5477-5485, https://doi.org/10.1093/mnras/sty943

Packham C. and the Canaricam instrument team: CANARICAM astronomers user manual

Pérez-Jordán G., Castro-Almazán J. A., Muñoz-Tuñón C., Codina B., Vernin J., 2015, Monthly Notices of the Royal Astronomical Society, 452, 1992

Reach W.T., Morris P., Boulanger F., Okumura K., The mid-infrared spectrum of the zodiacal and exozodiacal light, Icarus, Elsevier, august 2003.

Skamarock, W. C., J. B. Klemp, J. Dudhia, D. O. Gill, D. M. Barker, M. G Duda, X.-Y. Huang, W. Wang, and J. G. Powers, 2008: A Description of the Advanced Research WRF Version 3. NCAR Tech. Note NCAR/TN-475+STR, 113 pp.doi:10.5065/D68S4MVH

Telesco C.M., Ciardi D., FrenchJ., et al.,2003, CanariCam: a multimode mid-infrared camera for the Gran Telescopio Canarias, in SPIE Conference Series,Vol. 4841, 913

Vives-Arias H., Muñoz J.A., Kochanek C.S., MEdiavilla E., Jiménez-Vicente J., Observations of the Lensed Quasar Q2237+0305 with CanariCam at GTC, 2016

CANARICAM website: http://www.gtc.iac.es/instruments/canaricam/canaricam.php

IAC Site Testing website: http://www.iac.es/proyecto/site-testing/

IAC FOR-O PWV Forecasting system: http://vivaldi.ll.iac.es/proyecto/site-testing/index.php?option=com_wrapper&Itemid=148

CANARICAM Exposure Time Calculator:

http://gtc-phase2.gtc.iac.es:8080/itc/itc/servlets/ITCcanaricam.html

Grid Analysis and Display System (GrADS): http://cola.gmu.edu/grads/

WRF model user's page: http://www2.mmm.ucar.edu/wrf/users/

Colormaps (Ted Letcher): http://gradsaddict.blogspot.com/2014/05/script-colormapsgs-very-easily-create.html

12 Acknowledgements

First of all, I would like express my deepest agreements and huge thanks to my director, Casiana Muñoz Tuñón, for her help, guidance and advice in this work. She was always available for every doubt or concern I went through. I am also indebted to Julio Castro Almazán not only for providing one of the important datasets used in this work (the PWV from GPS monitor) but also for its useful advice and shared experience on statistics and water vapour.

I would also like to express my agreement to Antonio Cabrera, Head of Operations at Gran Telescopio Canarias, for his help in providing the necessary datasets from CANARICAM observation logs and also for his useful advice and comments. Also to Carlos Álvarez, for the useful sensitivity and flux data measured during CANARICAM commissioning and testing.

Finally I want to express the biggest thanks to my family, Pilar and Alex, as it was not always easy to find the balance between work and home life while preparing this project, but I had always their warmest support.